Frequencies and Thermal Stability of Isolated Surface Hydroxyls on Pyrogenic TiO_2 Nanoparticles

*Akbar Mahdavi-Shakib,[1,2,3,4†] Juan M. Arce-Ramos,[5†] Rachel N. Austin, [4] Thomas J. Schwartz,[1,2,6] Lars C. Grabow, [5] Brian G. Frederick[1,2,3]**

[1]Laboratory for Surface Science and Technology (LASST), [2]Forest Bioproducts Research Institute (FBRI), [3]Dept. of Chemistry, University of Maine, Orono, ME 04469.

[4]Dept. of Chemistry, Barnard College, Columbia University, New York, NY 10027

[5]Dept. of Chemical and Biomolecular Engineering, University of Houston 4726 Calhoun Rd., Houston, TX 77204-4004, USA

[6]Dept. of Chemical and Biomedical Engineering, University of Maine, Orono, ME 04469.

AUTHOR INFORMATION

*Corresponding Author

*B.G.F.: E-mail: briangf@maine.edu. Tel: (207) 581-2268.

†Authors made equal contributions

Abstract

The surface reactivity of TiO_2 is often governed by hydroxyl groups. Fourier transform infrared (FTIR) spectroscopy is the most commonly used method to study surface hydroxyls. However, interpretation of the observed bands of powder samples is not straightforward. In this work, we propose a facet-specific assignment of the surface hydroxyls of pyrogenic TiO_2 (commonly known as P25 and P90) by comparison between experimentally observed FTIR bands of P90, rutile, and anatase with calculated vibrational frequencies for well-defined surface facets using density functional theory (DFT). Titania was calcined for extended periods in extremely dry O_2 to remove carbonates and water for diffuse reflectance infrared spectroscopy (DRIFTS) measurements of the most thermally stable hydroxyls remaining in the 300 – 400 °C range. Reactions of the dehydroxylated surfaces with $H_2(D_2)$ provided further insight into hydroxyl formation. Theoretical assignments of hydroxyls were based on the calculated thermal stability of hydroxyls to dehydroxylation, agreement with calculated frequencies (scaled to be consistent with the experimental bridging hydroxyl frequency on rutile TiO_2(110)), and the thermodynamic stability of the specific facets. Our assignments, combined with previous results, show that terminal and bridging hydroxyl frequencies overlap; therefore, the common assumption that terminal hydroxyls vibrate at higher frequencies is not valid.

1. Introduction:

Titania is one of the most widely studied metal oxides,[1] with specific attention often given to the hydroxyl groups and their involvement in a variety of processes, including photocatalysis,[2-6] catalysis,[7-9] self-cleaning surfaces,[10-11] and bio-implants.[12] The reactivity of facets with water to form hydroxyls,[13-15] the type of hydroxyls formed,[16-20] and their surface acidity/basicity,[21-23] depend on the crystal phase as well as the detailed atomic structure and termination of TiO_2 facets. In catalysis, hydroxyls are particularly important because they are involved in surface grafting reactions,[8] and control both acidity[21, 24] and hydrophilic/hydrophobic interactions of adsorbates with the surface.[25] Although there is no clear relationship between frequency and acid strength,[24] titration experiments[26-27] allow hydroxyls of specific frequencies to be associated with their Brønsted acidic or basic character.[28] In photocatalysis, activity often increases with surface hydroxyl coverage.[29-30] Surface hydroxyls are proposed to be the adsorption sites for reactants[4] and their effect on electronic structure may affect the path through which electrons and holes migrate to the surface for photocatalytic reactions.[2, 5] There is much current interest in using oxide nanocrystals with controlled size, shape, and composition to relate the reactivity of specific facets with their reactivity in catalysis and photocatalysis.[31-36] The ability to associate vibrational frequencies with surface hydroxyls on specific facets of nanoparticles is necessary for an atomic level understanding of structure-function relationships in catalysis and materials design.

Pyrogenic titania is unique and widely used as a support in catalysis[37-38] and remains a defacto standard in photocatalysis.[6, 39-40] The P25 and P90 materials (Evonik; formerly Degussa) are synthesized by flash hydrolysis of $TiCl_4$ and contain individual anatase and rutile nanoparticles,[41-

[43] with typical composition 85-90% anatase and 10-15% rutile.[37, 43-46] Because of the high temperature preparation method, each particle is highly crystalline[42-43] and has few chemical impurities compared to TiO_2 samples prepared in the liquid phase.[37] Extensive efforts have been made to characterize the bulk and surface structure, morphology, and electronic structure.[5, 42-43, 45] However, fundamental understanding of the isolated hydroxyl groups is still lacking.[37]

Vibrational spectroscopy is a powerful method for characterizing hydroxyl groups and their role in surface reactions.[32, 47-48] The complexity of powder samples makes assigning the vibrational bands of surface oscillators challenging[37] because each crystallite is composed of multiple surface facets, the relative abundance of which change with sample preparation,[49] the local environment,[20, 43] and hydrogen bonding interactions with adsorbed water.[16, 44] Reports published over the past 50 years show that frequencies of the isolated hydroxyls are reproducible within a few wavenumbers (cm^{-1}) when contamination with hydrocarbons, carbonates, and water is excluded (See Supporting Information). [4-5, 50-54] Pyrogenic titania has three bands at 3718, 3673, and 3641 cm^{-1} that are typically attributed to anatase and two bands at 3687 and 3660 cm^{-1} that are attributed to rutile.

Assignments in the literature continue to be based on early proposals by Primet *et al.*[50] and Tsyganenko *et al.*[51] that terminal hydroxyls vibrate at higher frequencies than bridging hydroxyls. These assignments were qualitative and based on classical mechanics; however, recent DFT studies provide examples where the frequencies of terminal hydroxyls are lower than those of bridging hydroxyls.[55-56] Chizallet *et al.*[57] calculated the frequencies of terminal hydroxyls on anatase TiO_2 and bridging hydroxyls on MgO. They concluded that there is no correlation between hydroxyl frequencies and the oxygen coordination (i.e. bridging vs. terminal), although a clear relationship exists between frequency and bond length.[57] Hence, fundamental facet-specific studies are necessary for the proper assignment of the surface hydroxyls. Assignments based on

experimental work using well-characterized single crystals of TiO_2 are limited to the rutile (110) surface,[16-18, 44, 58] for a number of reasons discussed in the Supporting Information.

Arrouvel *et al.*[20] approached the assignment of the surface hydroxyls on anatase TiO_2 nanopowders in a unique way. They used DFT and statistical thermodynamic calculations to predict the type, frequency, and thermal stability of the surface hydroxyls that are formed by water dissociation on the anatase surfaces and reported the vibrational frequency of a number of terminal hydroxyls.[20, 57] The anatase (001) and (110) surfaces dissociate water upon adsorption regardless of surface coverage, while water dissociation on the anatase (100) surface occurs only at low coverages. Surface hydroxyls were not considered for the anatase (101) facet because this surface does not dissociate water in the defect-free state.[15] However, both theoretical[59-60] and experimental[61] work show that bridging hydroxyls form by dissociative adsorption of water on surface defects (*e.g.*, oxygen vacancies) of less reactive surfaces such as anatase (101).

In this work, we have extended the approach of Arrouvel *et al.* approach to consider the hydroxyls that are formed by water dissociation on surface oxygen vacancies of less reactive surfaces such as anatase (101) and rutile (110). Using DRIFTS experiments coupled with our calculations and information from the literature, we verified the spectral behavior of the surface hydroxyl bands of pyrogenic TiO_2 (P90), anatase, and rutile particles. We developed methods to obtain chemically clean surfaces under rigorously dry conditions and measured the infrared spectra of the most thermally stable, isolated surface hydroxyls on the TiO_2 samples. For the DFT-based assignment of the observed bands, we calculated the vibrational frequency and energetics of hydroxyls on the anatase (001), anatase (101), and rutile (110) surfaces. We present assignments of hydroxyl frequencies based on: 1) scaling the DFT calculated values to agree with experimental evidence from rutile (110) single crystals; 2) consistency with the observed thermal stability of the

surface hydroxyls; and 3) the thermodynamic and/or kinetic stability of the particular hydroxylated facet. We propose that the pyrogenic TiO_2 band at 3673 cm^{-1} is due to vibrations of the bridging hydroxyls on the anatase (101) surface, the 3687 cm^{-1} band is due to vibrations of the bridging hydroxyls on the rutile (110) surface, and the 3718 cm^{-1} band is due to vibrations of the terminal hydroxyls on the anatase (001) surface. Note that the high frequency hydroxyl at 3687 cm^{-1} on rutile (110) is of a bridging nature rather than a terminal hydroxyl as previously assumed. In addition, the hydrogen bonded hydroxyl formed by hydrolysis of the anatase (001) surface is calculated to be near 2850 cm^{-1}, despite being a terminal hydroxyl. These results, together with previous data,[20, 55-57] provide additional evidence that there is no correlation between hydroxyl frequencies and the oxygen coordination (i.e. bridging vs. terminal), although there is a statistically significant relationship between frequency and bond length.

2. Methods

2.1 Experimental

Three TiO_2 samples were studied in this work, which have been characterized for surface (XPS) and bulk (ICP-OES) elemental composition, specific surface area and crystal phase, as reported previously.[25] Pyrogenic TiO_2 (P90) was purchased from Evonik and used as-received. Rutile was purchased from US Research Nanomaterials and used as-received. Commercially available anatase samples contain sulfate impurities,[25, 62] which complicates the interpretation of spectral results, so we synthesized sulfate-free anatase using a modified sol-gel method described elsewhere.[63] Briefly, to 50 ml 100% ethanol in a 100 ml three-neck round-bottom flask in ice, we added 2.89 ml of $TiCl_4$ dropwise with a pressure equalized addition funnel. Once addition of $TiCl_4$ was

completed, the reaction was stirred at ambient condition for 2 hours. The reaction mixture was placed in an oven at 87 °C and heated for three days. The powder was rinsed by addition of MilliQ water and centrifuged at 20,000 rpm for 30 minutes, several times every day for 30 days until the pH of the supernate was around 7.

The bulk crystal phase of the rutile, sulfate-free anatase, and P90 (87% anatase, 13% rutile) materials was confirmed with x-ray diffraction[62] and pair distribution analysis.[46] The specific surface areas (P90 100 m^2/g; rutile 30 m^2/g; sulfate-free anatase 159 m^2/g) were reported in previous work.[25]

DRIFT spectra were recorded using a Nicolet 6700 Fourier Transform Infrared (FTIR) spectrometer equipped with a Praying Mantis™ (Harrick Scientific Production, IBC) accessory for DRIFTS applications. KBr powder was placed in the sample cup inside a Harrick Scientific high temperature reaction chamber (HVC). The HVC sample cup is located on a temperature-controlled sample stage equipped with a cartridge heater and a chromel-alumel (K-type) thermocouple. The temperature of the sample cup is controlled by a Harrick Scientific Automatic Temperature controller (ATC-024-1).

The TiO_2 samples were spread on the top of KBr powder in the sample cup for DRIFTS studies. After each material spread on KBr (or just KBr as reference) was loaded in the chamber, the environmental chamber was heated to 70 °C overnight under O_2 (Grade 2, Matheson) flow, and dried to achieve extremely low water vapor pressures.[62] Water and carbon dioxide impurities in the O_2 were removed using a molecular sieve trap (13X, 4 to 8 mesh, Acros Organic, degassed at 200 °C for at least one day) immersed in a dry ice-acetone bath. All DRIFTS spectra were recorded by accumulation of 512 scans at 8 cm^{-1} resolution using a DTGS detector.

2.2 Theoretical

Density functional theory (DFT) calculations were carried out using the Vienna Ab-initio Simulation Package (VASP) in combination with the Atomic Simulation Environment (ASE).[64-67] The projector augmented wave (PAW)[68] method and the generalized gradient approximation (GGA) with the revised Perdew−Burke−Ernzerhoff (RPBE) functional were employed to solve the Kohn−Sham equations.[69-70] All DFT calculations were performed with a cutoff energy of 680 eV and the tetrahedron method with Blöch corrections was used to treat the partial occupancies.[71] To correct for on-site Coulombic interaction of electrons in the localized Ti 3d state, we used the DFT+U approach by Dudarev *et al.* [72] with U_{eff} = 2.0 eV adopted from Hu and Metiu.[73]

The optimized lattice constants for both rutile and anatase bulk crystals are shown in Table 1 and agree well with those reported experimentally.[74-76] The rutile TiO_2(110) surface was represented with a 3×1 periodic unit cell, while for the (101) and (001) surfaces of anatase periodic cells of size 1×2 and 2×2 were used, respectively. Four-layer models were used in the rutile (110) and anatase (101) surfaces, while a five-layer model was adopted for the anatase (001) surface to maintain a consistent thickness of relaxed slab atoms. In all cases, the bottom two layers were kept fixed at optimized bulk positions and the top-most layers were allowed to relax. Periodic slabs were separated by 16 Å of vacuum space in the *z* direction and a dipole correction was applied to compensate for the effect of adsorbing molecules only on one side of the surface,[77] and spin polarization was included. The Brillouin zone was sampled using Monkhorst−Pack meshes[78] of 4×6×1, 6×6×1 and 4×6×1 for the rutile (110), (001) and (101) anatase surfaces, respectively. The atomic positions were optimized using a tight force convergence criterion of 0.02 eV/ Å.

Oxygen vacancy formation energies are reported with respect to gas phase O_2; its energy was calculated from the DFT values for H_2O(g) and H_2(g) using the tabulated heat of formation for water.

Vibrational modes and infrared intensities of surface hydroxyl groups were obtained using the finite differences method and harmonic oscillator approximation as implemented in the ASE package.[79] Only the hydrogen and directly-bound oxygen atoms of the hydroxyl groups were displaced in the positive and negative directions along the three axes and an energy convergence criterion of 1×10^{-8} eV was used to obtain sufficiently accurate first derivatives of energy while approximating the Hessian matrix. The effect of including displacements of nearest neighbor Ti atoms on the OH stretching frequencies, for selected bridging hydroxyls, was less than 0.1 cm^{-1}.

Table 1. Rutile and anatase TiO_2 lattice parameters used in this study.

Phase	*a*	*c*
Rutile (calc)	4.712	3.016
Rutile (exp) [a]	4.594	2.959
Anatase (calc)	3.872	9.783
Anatase (exp)[b]	3.785	9.512

[a] Morgan, *et al.*[75]

[b] Arlt, *et al.*[74]

3. Results

3.1 Pretreatment of materials

Spectra presented in Figure 1 show the systematic elimination of water, carbonate, bicarbonate and sulfate species that are commonly present on TiO_2 surfaces[37] and may account for

contradictory results reported by different authors.[8] Step-wise temperature-programmed calcination of the samples from 30 °C to 400 °C in the environmental chamber was followed with DRIFTS for at least 8 hours under flowing dry oxygen at each temperature until no further changes in the spectra were observed. The final spectra at each temperature, shown in Figure 1, were used to guide the pretreatment of materials prior to H_2/D_2 exchange experiments (Sect. 3.3).

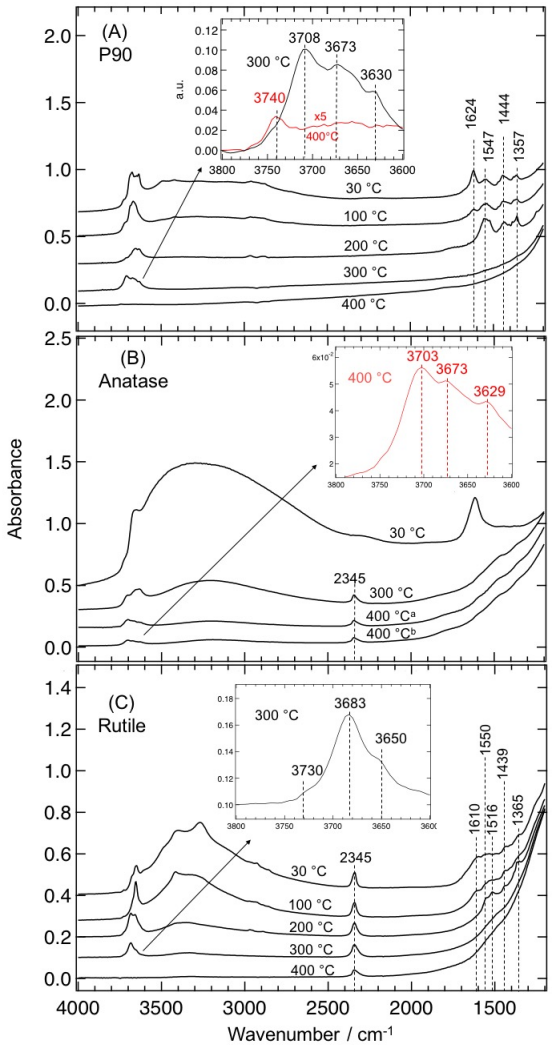

Figure 1. DRIFTS spectra of the TiO_2 samples, (A) P90, (B) anatase, and (C) rutile recorded during stepwise temperature programmed calcination from 30 to 400°C, as indicated. [a]Heated at 400 °C for one day, [b]heated at 400 °C for three days. Inset shows the DRIFTS spectra of the hydroxyls observed at indicated temperatures.

The DRIFTS spectrum of P90 recorded at room temperature (Figure 1A) contained several absorbances caused by surface impurities. The bands at 1357, 1444, and 1547 cm^{-1} are assigned to carbonate and bicarbonate species.[23] The 1624 cm^{-1} band is assigned to the bending mode of molecularly adsorbed water.[16, 49] The broad absorption in the 2500-3600 cm^{-1} region is characteristic of hydrogen bonded surface hydroxyls and hydrogen bonded water molecules. The complex feature in the 3600-3800 cm^{-1} region is characteristic of surface hydroxyl groups and water molecules coordinated to Lewis acid sites.[20, 49]

DRIFTS spectra showed that the surface is dehydrated at 200 °C, as evidenced by the elimination of the water bending band and the broad absorption feature in the 2500-3600 cm^{-1} region (Figure 1A), which is consistent with previous reports.[4, 20] The carbonate bands were eliminated from the spectrum at 300 °C. The 3708 cm^{-1} band grew in intensity as the surface impurities were removed at 300 °C. At the end, only three significant bands were resolved in the isolated hydroxyl region at 3630, 3673, and 3708 cm^{-1}. After overnight calcination at 400 °C, these bands were largely eliminated from the spectra, and only a small band at ~ 3740 cm^{-1} was observed (inset of Figure 1A). The vibrational frequency and high thermal stability of the latter band is consistent with previous assignments of this band to silica impurities.[80-81] This assignment is also supported by XPS analysis of P90, which shows the presence of silica impurities.[25] Thus, the P90 surface remained contaminated at temperatures below 300 °C and was dehydroxylated by 400 °C. In general, the dehydroxylation temperature will depend on the partial pressure of water and is different for each crystallographic facet (*vide infra*). Under the conditions used in this study, 300 °C was considered optimal for identifying the most thermally stable hydroxyls on chemically clean surfaces.

Because pyrogenic TiO_2 consists of individual anatase and rutile particles, samples of pure anatase and rutile were evaluated as well. Similar step-wise temperature-programmed calcination experiments were performed for the anatase (Figure 1B) and rutile (Figure 1C) samples. At room temperature, the DRIFTS spectrum of anatase shows strong absorbance in the 2500-3600 cm^{-1} region, indicating that the surface is highly hydroxylated making it hydrophilic and therefore retaining molecular water, as confirmed by the strong bending mode (~1620 cm^{-1}) (Figure 1B). Calcination at higher temperatures led to a reduction in the broad absorption feature in the 2600-3600 cm^{-1} region. However, this feature was not eliminated even after several days of calcination at 400 °C, in contrast to P90. Isolated hydroxyl bands at 3703, 3673, and 3629 cm^{-1} also persisted in the spectra during the calcination at 400 °C, which we will refer to as hydroxyl bands A1, A2, and A3, respectively. These bands must be due to surface hydroxyls because the water bending band was eliminated at 200 °C. The differences in hydroxylation between anatase and P90 may be due to the synthesis methods for each. It is known that the surface of TiO_2 samples prepared at low temperature in the presence of water, i.e. during the hydrolysis of $TiCl_4$, are extensively hydroxylated. While such surfaces undergo irreversible dehydroxylation during drying, some hydroxyls persist on the surface and remain even after evacuation at 700 °C.[37] Conversely, the surface of TiO_2 samples prepared at high temperature in the absence of water (*e.g.*, P90) are largely dehydroxylated as-synthesized.[37]

DRIFTS spectra recorded during the step-wise temperature-programmed calcination of rutile are shown in Figure 1C. Water and carbonate bands were eliminated from rutile after overnight calcination at 300 °C, while a broad H-bonded surface hydroxyl feature in the 2500-3600 cm^{-1} region and three isolated hydroxyls at 3730, 3683, and 3650 cm^{-1} remained (See inset of Figure 1C). Similar bands were previously reported for rutile powder samples.[50, 82-83] The band at 3730

cm^{-1} is consistent with assignment of this band to silica impurities[80-81] and is supported by XPS analysis.[25] We refer to the 3683 and 3650 cm^{-1} bands as R1 and R2, respectively. The isolated hydroxyl bands were eliminated after overnight calcination at 400 °C.

There was a band at 2345 cm^{-1} which appeared in the DRIFTS spectra of anatase and rutile, but not in the spectra of P90, and it persisted after overnight calcination at 400 °C. While this band could be due to the asymmetric stretching mode of linear CO_2 molecules coordinated to Lewis acid sites on the TiO_2 surface,[23] CO_2 molecules coordinated to Ti^{4+} sites persist on the surface at room temperature only under CO_2 atmosphere.[23] Hence, this band must have originated from the CO_2 molecules trapped in the structure, as previously reported for silica.[84]

3.2 Temperature dependence of hydroxyl bands

Figure 2 shows the DRIFTS spectra of the TiO_2 samples recorded at 300 °C and after the samples were returned to room temperature under dry O_2 flow. For P90, the decrease in temperature led to: an increase in the intensity of the $\upsilon\ (O-H)$ bands; blue shifts of the A1 and A3 bands at 3708 and 3630 cm^{-1} by 10 and 11 cm^{-1}, respectively; no change in the frequency of the A2 band at 3673 cm^{-1}; and better resolution of the R1 band at 3687 cm^{-1} from other absorbances. The R1 band was not resolved from the other bands in the 300 °C spectrum. The anatase TiO_2 sample behaved similarly to the P90 sample, except that the R1 band (3687 cm^{-1}) was absent (Figure 2B). The intensity of the R1 and R2 bands increased for the rutile TiO_2 sample and the absorbances at 3683 and 3650 cm^{-1} blue shifted by ~12 and 10 cm^{-1}, respectively (Figure 2C).

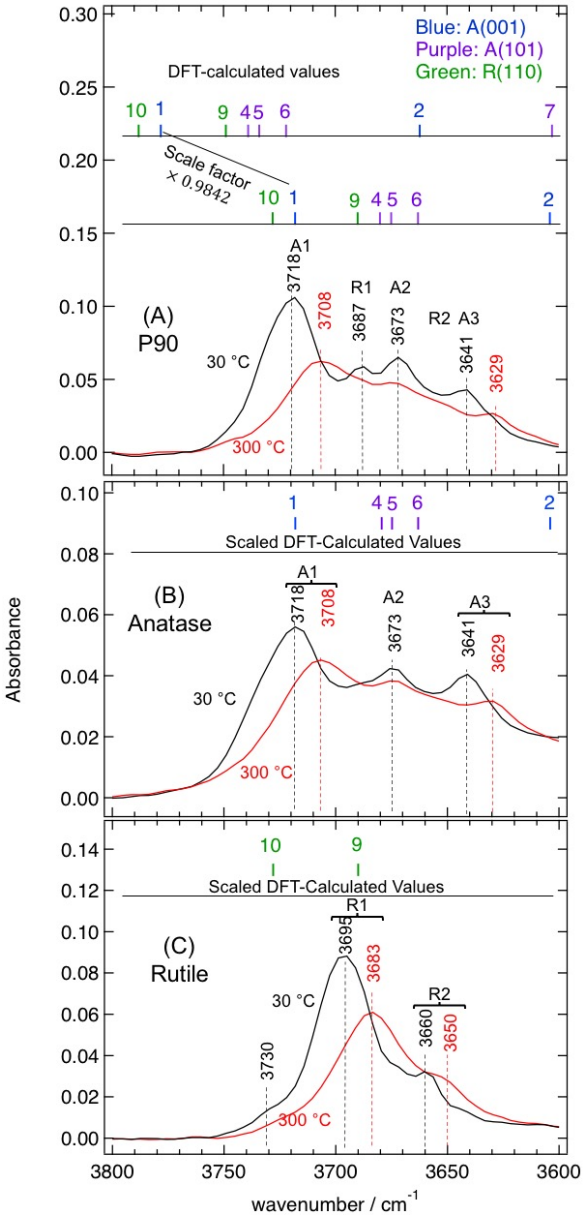

Figure 2. DRIFTS spectra of A) P90, B) anatase, and C) rutile in the hydroxyl region recorded at 300 °C (red spectra) and after cooling to 30 °C in rigorously dry O_2 (black spectra). Numbers along the top of part (A) show the DFT-calculated vibrational frequency of hydroxyls on the anatase (001) surface (blue), anatase (101) surface (purple), and rutile (110) surface (green), as summarized in Table 2. Numbers along the top of parts (A), (B) and (C) show the predicted vibrational frequencies of anatase and rutile hydroxyls after scaling the DFT-calculated values (see Discussion).

The spectral behaviors of the surface hydroxyls of pyrogenic TiO_2 P90 collected in this work compare well with information available in the literature for P25. A summary of the $\upsilon\ (O-H)$ values from the literature for P25 pyrogenic TiO_2 samples observed on reasonably dry surfaces is presented in the first five columns of Table 2, illustrating the lab-to-lab reproducibility of the measured frequencies. As others have shown,[5, 54] prior pretreatment at higher temperatures is required to observe the intrinsic surface hydroxyl bands of TiO_2 and, as described above, the surface hydroxyl region changed significantly at 300 °C when carbonate species were eliminated. Two of the $\upsilon\ (O-H)$ frequencies observed in this study for P90 at 300 °C (3630 and 3708 cm^{-1}) are slightly lower than those reported for P25 in Table 2. However, the reported P25 values summarized in Table 2 were recorded at room temperature, after initial pretreatment at higher temperatures. Spectra recorded at 300 °C were at a sufficiently high temperature to prevent adsorption of water on the surface, but under our conditions negligible uptake of water occurred during cooling to 30 °C and recording the spectra. The values of $\upsilon\ (O-H)$ measured for P90 at 30 °C were consistent with other values reported for P25 within ±2 cm^{-1}.

Table 2. Comparison of $\boldsymbol{\upsilon}$ $(\boldsymbol{O-H})$ values of the pyrogenic TiO_2 P25 with P90.

P25					P90			
Panayotov[52]	Lobo-Lapidus[53]	Nanayakkara[4]	Deiana[5]	Lin[54]	This Work (300 °C)	This Work (30 °C)	Regenerates by H_2 adsorption?	Assignment
-	-	3733	3736	3734	3740	3740		SiO_2
3716	3717	3717	3717	3715	3708	3718	no	A1; OH_{tr} A(001)
3688	3689	3691	3688	3688	-	3687	yes	R1; OH_{br} R(110)
3674	3672	3672	3672	3671	3673	3673	yes	A2; OH_{br} A(101)
3660	-	-	3659	3658	3650	3660	yes	R2; Rutile
3648	3642	3642	3642	3640	3630	3641	yes	A3; Anatase

3.3 Hydroxyls formed by reaction of TiO_2 with H_2 (D_2)

To demonstrate the formation of surface hydroxyls from dissociation of H_2 independent of the adsorption of background water, we performed our experiments under rigorously dry conditions and at 300 °C. Before exposure to H_2, we cleaned the TiO_2 samples by calcination at 400 °C under dry O_2 for at least 8 h. The state of the surface after such pretreatment can be assessed from the spectra depicted in Figure 1. We achieved highly dehydroxylated surfaces for P90 and rutile with no detectable impurities, except for traces of SiO_2, but the anatase sample remained slightly hydroxylated. Spectra depicted in Figure 3 were recorded during the reaction of such surfaces with H_2 at 300 °C. By comparison with Figure 2, H_2 dissociated to form only certain hydroxyls. Reaction of the P90 surface with H_2 at 300 °C regenerated only the two hydroxyl bands A2 and A3 at 3673 and 3645 cm^{-1} (Figure 3A). The anatase spectrum still contained three bands at 3630, 3673, and 3708 cm^{-1} after calcination at 400 °C, and cooling to 300 °C before exposure to H_2 but,

as the difference spectrum in Figure 3B shows, only the two overlapping A2 and A3 bands regenerate upon H_2 exposure. These are the same bands as found for P90, which is consistent with ~87% anatase content of P90 determined in total scattering x-ray diffraction measurements.[46] Reaction of the dehydroxylated rutile surface with H_2 regenerated the two bands (R1 and R2) at 3683 and 3655 cm^{-1}, which were stable to 300 °C during dehydroxylation. The bands that increase after exposure to H_2 are summarized also in Table 2.

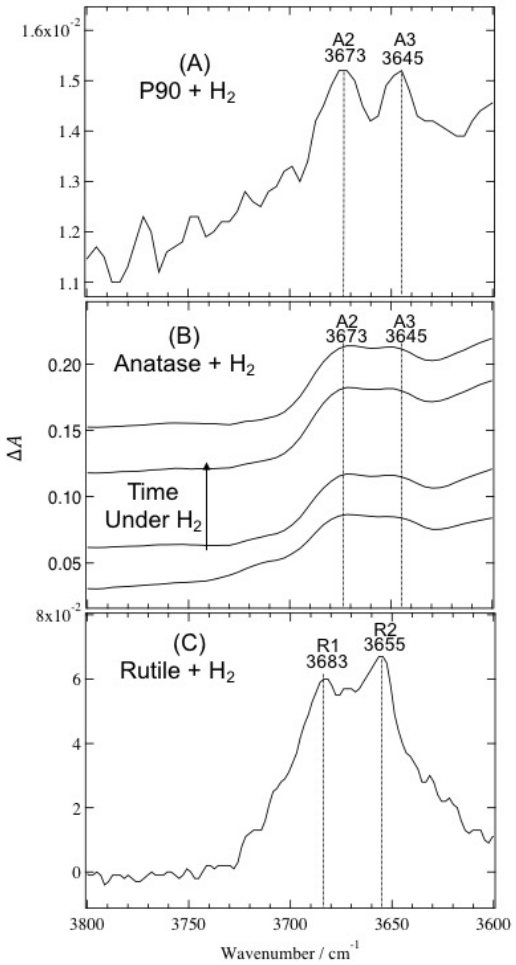

Figure 3. Difference DRIFTS spectra of A) P90, B) anatase, and C) rutile in the hydroxyl region recorded during the reaction of the 400 °C pretreated TiO_2 samples with H_2 at 300 °C. All the spectra are relative to the DRIFTS spectrum of the sample recorded under Ar at 300 °C right before exposure to H_2.

Previous reports show that H_2 dissociates on pyrogenic titania (P25) above 250 °C to yield electrons and protons.[85] The protons bond to surface oxygens (to form hydroxyls) and the electrons accumulate in the CB and mid-gap states.[86-88] We observed a broad electronic absorbance feature and hydroxyl stretching bands for all these samples after reaction with H_2 at 300 °C.[62] The increasing background with time of reaction with H_2 is illustrated in Figure 3 B for anatase.

Reaction of the hydroxylated anatase surface with D_2 gave further insight into how surface hydroxyls are preferentially formed upon hydrogenation. Figure 4A shows that, in addition to a broad electronic absorption with a threshold at 1000 cm^{-1} and extending beyond 7000 cm^{-1}, H/D exchange resulted in negative-going bands in the OH region and positive-going bands in the OD region. Comparison of the expanded spectra in Figures 4B and C shows that initially, the relative intensities of the negative-going OH bands are similar to the corresponding positive-going OD bands. After isotopic substitution, the relative intensity of the negative-going OH bands remained unchanged during the reaction, although they shifted upwards due to the increasing electronic absorbance background. However, at longer times, the relative intensity of the 2704 cm^{-1} OD band increased, indicating that hydroxyl formation occurred only on specific facets or type of surface oxygens (corresponding to the A2 and A3 hydroxyls). The continuous growth of the broad electronic absorption feature implies a continuous addition of electrons to the shallow trap states of anatase TiO_2 [62] as OD groups were formed and then dehydroxylated to produce oxygen vacancies. The hydroxyl stretch intensity monitors the OD intermediate coverage, which reaches steady state within minutes.

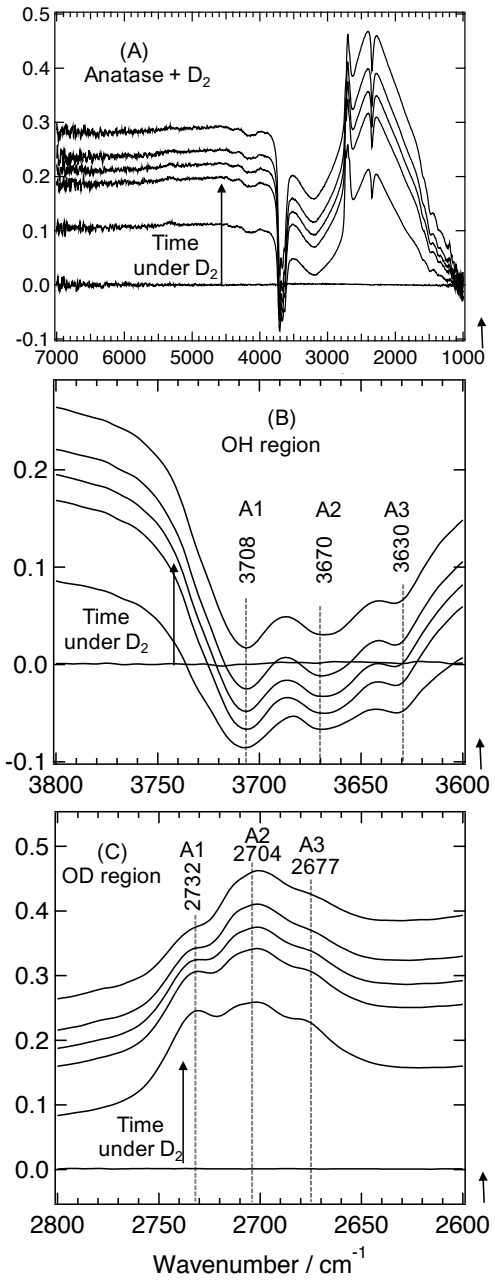

Figure 4. Difference DRIFTS spectra recorded during the reaction of anatase with D_2 at 300 °C. (A) overall spectra showing both vibrational and broad electronic absorbance features upon the reaction with D_2 and H/D exchange; (B) OH region showing negative-going bands and (C) OD region showing that in addition to the initial H/D exchange, the band at 2704 cm^{-1} continues to grow, which corresponds to the hydroxyl at 3673 cm^{-1}.

3.4 DFT calculations

We consider three pathways involved in the formation and loss of surface hydroxyls, illustrated schematically in Figure 5. First, water dissociation on the stoichiometric surface, via hydrolysis of a Ti-O bond, results in two terminal hydroxyls, which has been investigated extensively by Arrouvel *et al.*[20] for the anatase (001), (100), (110), and (101) surfaces. They calculated surface free energies and predicted phase diagrams to estimate the equilibrium coverage of hydroxyls as a function of temperature and water vapor pressure. Second, dissociation of H_2 on the stoichiometric surface can produce terminal or bridging hydroxyls, depending on the face and termination. Third, dissociation of water at a surface oxygen vacancy site can produce a pair of bridging hydroxyls. Note that the hydroxylated surface in the second and third pathways is nominally the same, with two electrons produced during reduction that may be formally represented as localized on the titanium ions as Ti^{3+} (See Supporting Information for more details). Bridging hydroxyls were not considered in Arrouvel's work.[20] Our work reproduces the terminal hydroxyls on the (001) face of anatase (for direct comparison of frequencies between methods) and augments their data with DFT calculations of bridging hydroxyls on the (101) and (001) faces of anatase and the (110) face of rutile to assess the thermal stability and estimate the vibrational frequencies. Experimentally, the surfaces are hydroxylated as received; therefore, loss of hydroxyls may be limited either by thermodynamic differences or by activation energy barriers. The structures of the stoichiometric surface and surfaces after creation of an oxygen vacancy on the (101) and (001) faces of anatase are shown in the Supporting Information Figure S1. The structures and vacancy creation energies are in good agreement with previous calculations.

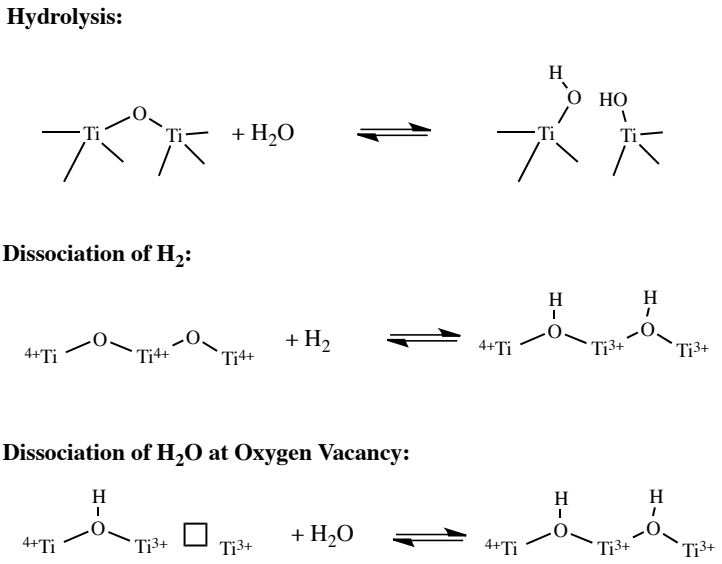

Figure 5. Schematic pathways for formation and dehydroxylation of surfaces: 1) dissociative adsorption of water on stoichiometric surfaces by hydrolysis to form terminal hydroxyls; 2) dissociative adsorption of H_2 on stoichiometric surfaces by hydrolysis to form bridging hydroxyls; and 3) dissociative adsorption of water at a surface oxygen vacancy to form bridging hydroxyls. Two electrons produced by reduction in pathways 2 and 3 are formally represented as Ti^{3+}.

3.4.1 Thermal stability

Figure 6A shows two adjacent terminal hydroxyls produced by dissociative adsorption of H_2O via hydrolysis on the stoichiometric (001) face. These H-acceptor and H-donor hydroxyls are referenced throughout the document with the respective identification numbers **1** and **8**. This configuration has a hydroxyl coverage of $\theta = \frac{n_H}{(n_{O_{2c}} + n_{O_{3c}})} = 0.25$, where the coverage θ is defined as the number of H atoms, n_H, divided by the sum of 2- and 3-fold coordinated oxygen sites on the surface, $n_{O_{2c}}$ and $n_{O_{3c}}$. If water adsorbs dissociatively at a vacancy site on the (001) face, two bridging hydroxyl groups with $\theta = 0.25$ are formed, denoted as **2** and shown in Figure 6B. To study the influence of the local environment and quantify interactions between bridging hydroxyls

we also considered an isolated bridging hydroxyl as shown in Figure 6C ($\theta = 0.125$). Hydroxyl **5** indicates the location of the most stable isolated bridging hydroxyl for the (101) face is given in Figure 7A ($\theta = 0.083$), and two possible paired configurations of bridging hydroxyls with $\theta = 0.167$ are displayed in Figures 7B and 7C, hydroxyls **6**, **7**, and **4**. Both paired hydroxyl configurations represent final states of dissociative water adsorption over an oxygen vacancy site on the (101) face. The corresponding vibrational frequencies of the O–H stretching modes as calculated with DFT are presented in Table 3. For comparison to experimental and theoretical literature values, we also calculated the structures and frequencies of bridging hydroxyls on the rutile (110) surface at coverages corresponding to $\theta = 0.111$ and $\theta = 0.222$ (structures not shown).

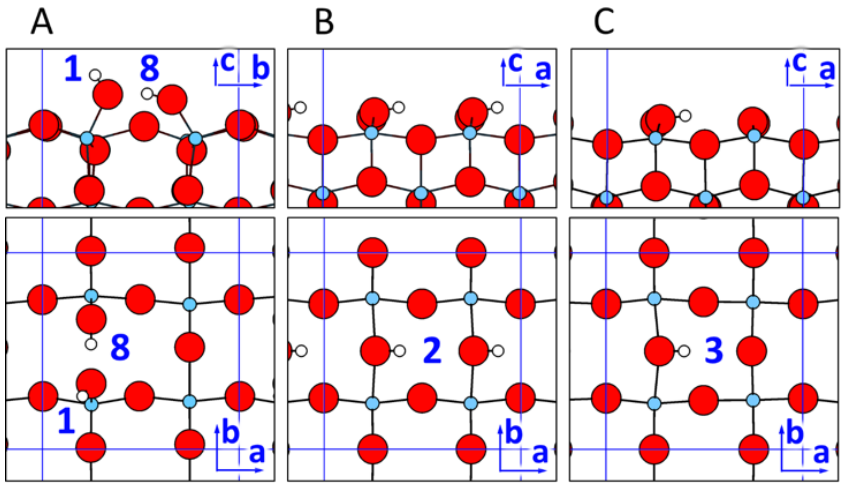

Figure 6. Hydroxylated surfaces of the (001) face of anatase. A) Water dissociation via hydrolysis of the stoichiometric surface to form two terminal hydroxyl groups at O_{1c} sites; B) water adsorption onto a surface oxygen vacancy or H_2 dissociation on the stoichiometric surface to form two bridging hydroxyls at O_{2c} sites; and C) a single bridging hydroxyl at the O_{2c} site. Ti, O, and H atoms are shown in blue, red, and small white circles, respectively. Only surface atoms are shown in the top view for clarity. Limits of the periodic cell are shown with blue lines.

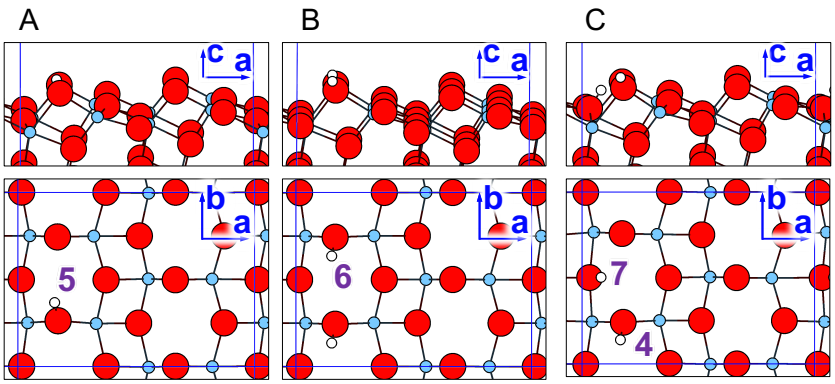

Figure 7. Hydroxylated surfaces of the (101) face of anatase. A) a single bridging hydroxyl at the O_{2C} site; B) water adsorption onto a surface oxygen vacancy or dissociation of H_2 on the stoichiometric surface to form two bridging hydroxyls at O_{2c} sites; C) same as B) but with one proton moved to the adjacent O_{3c} site. Only surface atoms are shown in the top view for clarity. The atom color code is the same as in Figure 6.

To estimate the thermal stability of various surface hydroxyls on anatase (001) and (101) at elevated temperatures we have calculated their Gibbs free energy relative to the respective stoichiometric surface termination and the gas phase chemical potential of H_2 and H_2O. We calculated the gas phase chemical potential according to

$$\mu(T,P) = E_{DFT} + E_{ZPE} + \int_0^T C_p dT - TS(T) + kT \log\frac{P}{P_0},$$

where E_{DFT} represents the total electronic energy calculated from DFT, and E_{ZPE} is the vibrational zero point energy. To approximate the dry oxygen conditions of the DRIFTS experiments we use the known partial pressure of O_2 as 1 bar (equivalent to the standard pressure $P_0 \equiv 1bar$) and approximate the partial pressure of H_2O as 10^{-5} torr. Temperature dependent enthalpy and entropy contributions for gas-phase O_2 and H_2O were adopted from the NIST-JANAF thermochemical tables.[89] No corrections were applied to the surface energies and we expect hydroxyl stabilities to be underestimated given the lack of surface entropy. Notably, the stability assessments are made

without considering surface coverage or lateral interactions. With this assumption the stabilities of the sets of hydroxyls, {**1**, **8**}, {**2**, **3**} and {**4**, **5** and **6**} are identical. The full calculations are provided in the SI.

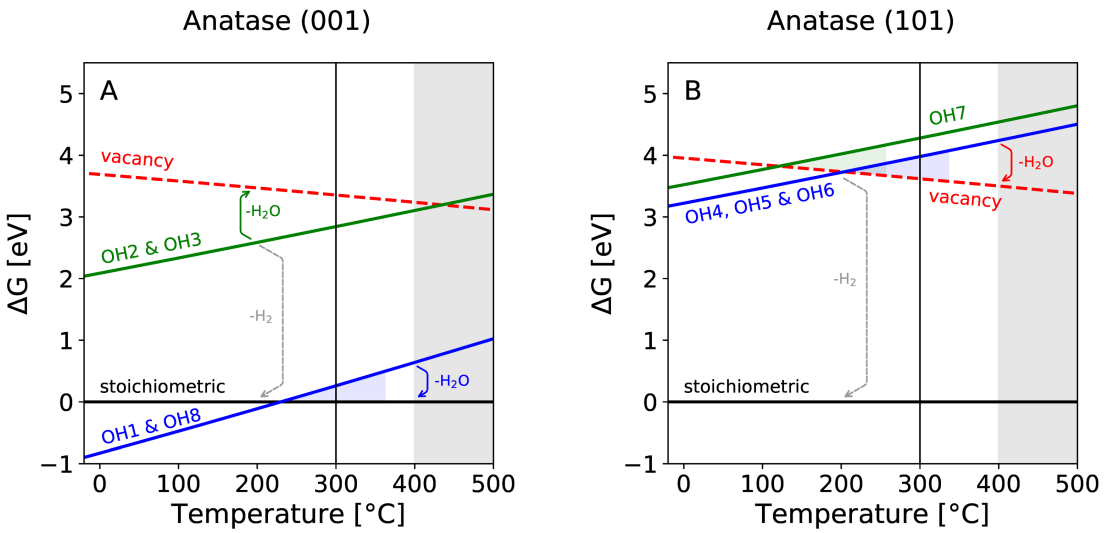

Figure 8. Temperature-dependent stability of surface hydroxyls at $p_{O_2} = 1$ bar and $p_{H_2O} = 10^{-5}$ torr. A) Gibbs free energy of hydroxyls **1**, **2**, **3** and **8** on anatase (001). B) Gibbs free energy of hydroxyls **4**, **5**, **6** and **7** on anatase (101). Gibbs free energies are reported with respect to the stoichiometric surface terminations. The vertical line at 300 °C indicates the temperature of our DRIFTS experiments and the gray shaded region above 400 °C represents conditions under which no hydroxyl frequencies were experimentally observable. The removal of hydroxyls by loss of H_2O or H_2 is illustrated with annotated arrows.

Given the low partial pressures of H_2O, Figure 8 shows that the stoichiometric termination is most stable at 300 °C for both anatase faces. When starting from a hydroxylated surface, however, one needs to consider the feasibility of reaching the stable stoichiometric configuration. Considering the terminal hydroxyls **1** and **8** as shown in Figure 6A as a starting point, there exists

a direct dehydroxylation pathway to the stoichiometric (001) face: 2 $HO_{1c} \rightarrow TiO_2(001) + H_2O(g)$. The Gibbs free energy change for this reaction at 300 °C can be quantified as the difference between the blue and black lines in Figure 8A. While the reaction at 300 °C is exergonic by $\Delta G_R = -0.26$ eV, cluster calculations find that water adsorption is non-activated on $TiO_2(001)$[90-91]. Therefore, we take the desorption barrier to be equal to the 0.7 eV energy difference, suggesting that the thermal energy at this temperature is insufficient to overcome the desorption barrier. Thus, we argue that the terminal hydroxyls are kinetically trapped on the anatase (001) surface, which we visually indicate as a light blue shaded triangle between the lines representing terminal hydroxyls and the stoichiometric surface in Figure 8A. The upper bound of the triangle was chosen as $\Delta G_R = -0.5$ eV, which is consistent with the disappearance of the corresponding frequency at temperatures in excess of 400 °C. The absence of any O-H stretch frequencies above 400 °C is expressed as a gray shaded area in Figure 8.

To reach the stoichiometric (001) termination from two pre-existing bridging hydroxyls **2** as shown in Figure 6B, the surface could undergo recombinative H_2 elimination: 2 $HO_{2c} \rightarrow TiO_2(001) + H_2(g)$. Various studies have reported this reaction to be highly activated with barriers on the order of ~2 eV on the (101) surface[92] and so we expect that the direct transition is unlikely. Instead, dehydroxylation to form a vacancy followed by healing of the vacancy is plausible and is shown as the difference between the green and red lines in Figure 8A. At 300 °C the Gibbs free energy change for the dehydroxylation process, 2 $HO_{2c} \rightarrow H_2O(g) + O_{2c,vac}$, is $\Delta G_R = +0.51$ eV. The endergonic nature of this step implies that there is no thermodynamic driving force to form the required vacancy site. Hydroxyl **3** is the low coverage version of hydroxyl **2** and we assume a similar stability for both. Overall, we argue that despite the thermodynamic stability of the stoichiometric anatase (001) face, both terminal and bridging hydroxyl species remain on the

surface at 300 °C when starting a temperature ramp from their hydroxylated counterparts at lower temperature.

For the (101) face of anatase we can immediately conclude from Figure 8B that hydroxyl **7** at the O_{3c} site is unstable compared to the bridging hydroxyls **4**, **5**, and **6** on O_{2c} sites, which we consider isoenergetic. For associative desorption of H_2 from the hydroxylated (101) face activation barriers in the range of 1.8 to 2.0 eV have been reported, allowing us to discard this pathway as kinetically limited.[92] As for the (001) face, we consider a two-step mechanism requiring the initial formation of a vacancy site by water elimination. While the Gibbs free energy change for dehydroxylation at 300 °C is exergonic with $\Delta G_R = -0.36$ eV, we again invoke a kinetic argument and postulate that up to $\Delta G_R \approx -0.5$ eV the dehydroxylation step is slow. The range of kinetically stabilized bridging hydroxyls on the (101) face is then depicted as the light blue triangle in Figure 8B between the blue and red line corresponding to bridging hydroxyls and the vacancy defect, respectively. To substantiate our assertion we refer to the desorption energy for 2 $HO_{2c} \rightarrow H_2O(g) + O_{2c,vac}$ at 0 K, which we obtained as 1.25 eV, consistent with the value of 1.2 eV reported by Aschauer and Selloni.[92]

3.4.2 Vibrational frequencies

The calculated bond lengths and vibrational frequencies of the TiO_2 hydroxyls studied in this work are summarized in Table 3.

Table 3. Calculated $\upsilon(O-H)$ and $\upsilon(O-D)$ on the (001) and (101) faces of anatase and rutile (110). Coverage of hydroxyl groups and O–H bond lengths are also included. Scaled frequencies shown in parentheses (See Discussion).

ID	Phase	Facet	Type	θ	Bond length $(O-H)$, Å	$\upsilon(O-H)$ cm^{-1}	$\upsilon(O-D)$ cm^{-1}
1	ana	(001)	O_{1c}–H	0.25	0.9710	3778 (3718)	2750
8	ana	(001)	O_{1c}–H	0.25	1.0107	2896 (2850)	2117
2	ana	(001)	O_{2c}–H	0.25	0.9777	3662 (3604)	2666
3	ana	(001)	O_{2c}–H	0.125	0.9814	3598 (3541)	2617
4	ana	(101)	O_{2c}–H	0.167	0.9733	3739 (3680)	2721
5	ana	(101)	O_{2c}–H	0.083	0.9740	3734 (3675)	2717
6	ana	(101)	O_{2c}–H	0.167	0.9743	3722 (3663)	2708
7	ana	(101)	O_{3c}–H	0.167	0.9801	3603 (3546)	2620
9	rut	(110)	O_{2c}–H	0.222	0.9717	3749 (3690)	2727
10	rut	(110)	O_{2c}–H	0.111	0.9701	3788 (3728)	2756

On the (001) facet, hydroxyls **1** and **8** (Figure 6A) are formed from water dissociation, as reported by Arrouvel *et al.*[20] During this process, a hydroxyl from water sits over a Ti_{5c} site while one lattice O_{2c}-Ti_{5c} bond breaks and forms an additional terminal hydroxyl (O_{1c}-H) with the remaining proton from water. The new OH groups are hydrogen-bonded to each other. While

hydroxyl **1** is a H-bond acceptor group, hydroxyl **8** is a H-bond donor. The donor and acceptor character of the OH groups change their bond lengths and, consequently, the corresponding vibrational frequencies. The calculated bond length of the terminal hydroxyls **1** and **8** are 0.971 and 1.011 Å and the corresponding calculated vibrational frequencies are 3778 and 2896 cm^{-1} respectively. Our frequency of 3778 cm^{-1} is higher than that of Arrouvel *et al.*[20] (3760 cm^{-1}), which we attribute to variations in the level of theory used in the DFT calculations and the inclusion of anharmonic corrections by Arrouvel *et al.* The unusually low frequency of 2896 cm^{-1} for the terminal hydroxyl **8** with H-bond donor character provides additional evidence that the classical assignment of lower frequency OH modes to bridging hydroxyls is not necessarily valid.

The critical influence of the local environment becomes evident upon further inspection of the calculated O–H stretching frequencies summarized in Table 3. On the (001) face, when the coverage of hydroxyls increases from $\theta = 0.125$ (hydroxyl **3**, Figure 6C) to a pair of equivalent hydroxyls with $\theta = 0.25$ (hydroxyl **2**, Figure 6B), the O–H bond length decreased from 0.981 Å to 0.978 Å and $\upsilon(O-H)$ increased from 3598 cm^{-1} to 3662 cm^{-1} (64 cm^{-1} blue shift). On the anatase (101) surface, the calculated $\upsilon(O-H)$ for the bridging hydroxyls (O_{2c}-H) were 3739 cm^{-1} (hydroxyl **4**, Figure 7C), 3734 cm^{-1} (hydroxyl **5**, Figure 7A) and 3722 cm^{-1} (hydroxyl **6**, Figure 7B). Notably, the increase of the hydroxylation coverage has a different effect on the $\upsilon(O-H)$ of the O_{2c}-H groups of the anatase (101) surface depending on the nature of the neighboring hydroxyl. For example, if we use hydroxyl **5** in Figure 7A with $\theta = 0.083$ as reference, a coverage increase to $\theta = 0.167$ by adding a neighboring O_{3c}-H (Figure 7C) causes a $\upsilon(O-H)$ blue shift by 5 cm^{-1}, while an adjacent O_{2c}-H (Figure 7B) produces a $\upsilon(O-H)$ red shift by 12 cm^{-1}. On the rutile (110) surface, the calculated frequency for an isolated hydroxyl at $\theta = 0.111$ (hydroxyl **10**, Table 3) is 3788 cm^{-1} and the calculated frequency for a pair of hydroxyls with $\theta = 0.222$ (hydroxyl **9**, Table

3) is 3749 cm^{-1}. Here, the presence of an adjacent O_{2c}-H group produces a $\upsilon(O-H)$ red shift by 39 cm^{-1} in the equivalent hydroxyls. Overall, our results suggest that depending on the local environment of hydroxyl groups their O-H stretch frequencies can exhibit substantial blue or red shifts. The strong dependence on coverage and the local environment makes robust band assignments challenging. Moreover, within the GGA+U approximation with U = 2 eV the excess electrons present after hydrogenation or water dissociation over a vacancy defect remain delocalized and potential frequency shifts resulting from localized electronic defects are not captured (Supplementary Information S.2.4).

4. Discussion

4.1 Previous assignments

Although there are many thermodynamic and structural studies of TiO_2 surfaces,[1, 14-15, 93-94] vibrational frequencies measured on single crystal surfaces and theoretical calculations are rare. A number of inconsistencies remain in the assignment of TiO_2 surface hydroxyls. Surface hydroxyl band assignments of anatase and rutile titania continue to be based on early coordination models of bridging vs. terminal hydroxyls and the assumption that terminal hydroxyls will have higher stretching frequencies than bridging hydroxyls. [8] Recent theoretical studies for goethite[56] and anatase[55] show that the original categorization of the high frequency bands to terminal hydroxyls and low frequency bands to bridging hydroxyls is not always correct. For example, Liu *et al.*[55] using DFT calculations reported that on the anatase (101) surface, bridging hydroxyls vibrate at 3727 cm^{-1} (similar to our hydroxyl 5 in Fig. 7B, 3734 cm^{-1}), while the frequency of a terminal hydroxyl on the coordinatively unsaturated Ti_{5c} site was 3627 cm^{-1}. Recently, Wei *et al.*[95] have calculated the frequency of Ti-H and bridging O-H vibrations for heterolytic dissociation of H_2 on

rutile (110), (100), (001), and (101) faces, and found that hydroxyl frequencies span from 2976 to 3743 cm^{-1}. Fundamental studies are required for assignment of surface hydroxyl bands.

Arrouvel *et al.*[20] made a significant advance towards the rational interpretation of the surface hydroxyl bands of anatase nanopowders by doing extensive calculations of the surface energies, vibrational frequencies, and phase diagrams (the relative surface energy of the hydrated surfaces and the oxygen-terminated surface as a function of temperature and partial pressure of water), which provide additional criteria for assignment of hydroxyls to specific facets. As expected, the frequency of water molecules coordinated to surface Lewis acid sites overlap with terminal surface hydroxyls,[20] which complicated several subsequent attempts to identify the isolated hydroxyls. Dzwigaj *et al.*[49] recorded FTIR spectra for anatase powders in the presence of several Torr of water vapor and compared the frequency of the hydroxyl bands with the DFT calculations of Arrouvel *et al.*[20] for well-defined anatase faces; however, bands that are typical of dry anatase titania (the 3673 and 3718 cm^{-1} bands, see Table 2) were identified as molecular water. As Deiana *et al.*[5] noted, the isolated hydroxyl frequency predictions of Arrouvel *et al.*[20] could not be confirmed because adsorbed water was present under the Dzwigaj experimental conditions and most hydroxyl stretching bands were assigned to adsorbed water. Although Deiana *et al.*[5] pretreated P25 up to 600 °C under vacuum conditions of 10^{-5} mbar, upon cooling to room temperature residual water readsorbed, which is clearly evident from the presence of the water bending mode, again precluding measurement of the isolated surface hydroxyls. Yet, Deiana *et al.* continued to assign isolated hydroxyl frequencies using the original assumptions of Primet *et al.* [50] and Tsyganenko.[51]

4.2 Frequency not correlated with oxygen coordination

Chizallet *et al.*[57] reviewed previous calculations of hydration energies and hydroxyl frequencies for dissociative adsorption of water on the more covalent oxides, anatase TiO_2 and Al_2O_3, and for the ionic oxide MgO. They categorized surface hydroxyls of metal oxides into three groups: H-bond donors, H-bond acceptors, and isolated hydroxyls. H-bond donor hydroxyls vibrate at lower frequencies, while isolated and hydrogen bond acceptor hydroxyls vibrate at higher frequencies.[57] Within hydrogen bond donors, there was no relationship between coordination of oxygen and the anharmonic frequency of the hydroxyl. Although they concluded that, among isolated and hydrogen bond acceptors, terminal hydroxyls generally vibrate at higher frequencies,[57] the effect of oxygen coordination vs. metal oxygen bond covalency (MgO vs. TiO_2) is not clear. Our calculations for bridging and terminal hydroxyl frequencies on TiO_2, shown in Figure 9 a, illustrate that the frequencies decrease linearly with the O–H bond length regardless of the coordination of the oxygen atom involved in the bond. Our TiO_2 data is combined with that of Arrouvel *et al.*[20] for anatase TiO_2 and Wei *et al.*[95] for rutile TiO_2 in Figure 9b. Differences in the density functional and computational methods result in systematic offsets between the data (see the Supporting Information for more details), but the linear dependence of frequency and bond length is clearly consistent. To compensate for differences in methods, the frequency of the bridging hydroxyl on rutile(110) for our work and that of Wei *et al*.[95] is scaled to the average single crystal value of 3686 cm^{-1}, while the common terminal hydroxyl structure on anatase (001) was used to align the frequencies of Arrouvel *et al.*[20] and this work. Terminal hydroxyls are shown as filled circles while bridging hydroxyls are represented as triangles. As indicated by the vertical double-ended arrows at the right side of Figure 9b, the range of bridging hydroxyl frequencies clearly overlaps the range of terminal hydroxyl frequencies. Thus, our data complement previous data[57, 95] for titania and make it clear that *there is no correlation between bridging and terminal OH frequencies*. Rather,

there is a strong relationship between the bond length and hydroxyl frequency, which depends on the local surface structure and bonding.

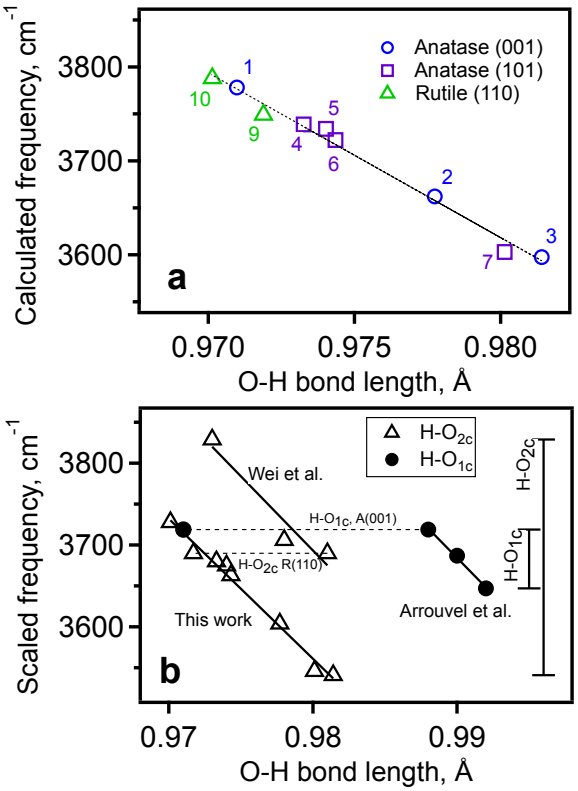

Figure 9. a) The O-H stretching frequency of surface hydroxyls as function of the O-H bond length Points labeled 1-7 correspond to the structures shown in Figures 6 and 7. Vibrational frequencies of bridging hydroxyls 9 and 10 over the (110) facet of rutile at two coverages (1/9 and 2/9) are also shown for comparison. **b**) Composite results from this work, Arrouvel *et al.*[20] for anatase and Wei *et al.*[95] for rutile illustrating the lack of correlation between frequency and oxygen coordination. Circles indicate frequency of terminal hydroxyls while triangles represent bridging hydroxyls. See text for details of DFT methods and scaling of frequencies for comparison.

4.3 Assignment of pyrogenic titania hydroxyls

To assign bands to specific hydroxyl groups, we employed three criteria: (a) thermodynamic stability of facets; (b) thermal stability of each type of hydroxyl; and (c) agreement between

experimental and scaled DFT frequencies. Although imposing several criteria should improve the confidence in assignments, we present our assignments here and give a critical assessment of the proposed method in section 4.4.

We begin assignment of the hydroxyls remaining after calcination at 300 °C by imposing the thermal stability constraint for anatase frequencies previously reported by Arrouvel *et al.*[20] Their phase diagrams that involve molecularly adsorbed water on anatase (100) and (101) have low thermal stability. We show the frequency of these bands as open boxes in Figure 10 to convey their low thermodynamic stability. Based on the calculated phase diagrams and the absence of water bending modes in our spectra, we can eliminate molecular water adsorption structures. For dissociative adsorption of water to form terminal hydroxyls, Arrouvel's phase diagrams indicate that hydroxyls on the anatase (001) and (110) surfaces satisfy the stability constraint (solid boxes), while those on the (100) do not (open box). Dzwigaj *et al.* [49] assigned a band at 3670 cm^{-1} to the molecular water mode on (101), which is the only potential assignment for the band we observe at 3673 cm^{-1} (designated A2). This would be inconsistent because there is no water bending mode in our spectra and water is predicted to desorb at lower temperatures.[20]

We extended Arrouvel's work by estimating thermodynamic and kinetic stabilities for hydroxyls formed on the anatase (101) and (001) surfaces. Our stability data at 300 °C suggest that the anatase (101) surface remains covered with bridging hydroxyls **4**, **5**, and **6**, and the anatase (001) surface is populated with the terminal hydroxyls **1** and **8**, as well as bridging hydroxyls **2** and **3**. These are shown as solid boxes in the bottom two rows of Figure 10.

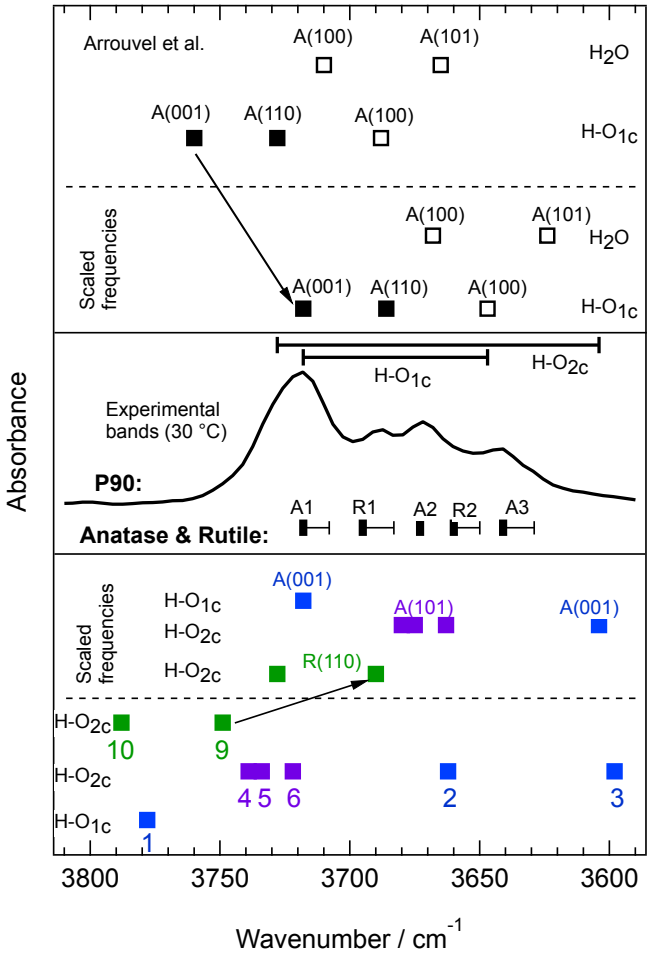

Figure 10. Assignment of the surface hydroxyl bands using the calculated vibrational frequencies and thermal stability calculated by Arrouvel *et al.*[20] and in this work. Arrouvel's values are shown above the P90 spectrum and our values are shown below, where blue and purple indicate anatase bands and green shows rutile bands. The filled symbols show the species that can exist on the surface at 300 °C and empty symbols show the species that will desorb from the surface at temperatures below 300 °C, based on the calculated stability diagrams. The range of the experimental values for A1-A3 and R1-R2 (shown as error bars below the IR spectrum) are based on the shift with increasing temperature of the observed bands in Figure 2. The ranges of OH_{tr} and OH_{br} indicate the range of scaled calculated frequencies from Figure 9b.

To make direct comparison between theoretical frequencies and experiment, we scale the DFT frequencies based on the bridging hydroxyls on rutile TiO_2(110), which is the only single crystal titanium dioxide surface for which hydroxyl frequencies have been measured. Values for surface hydroxyls generated from the reaction of water with oxygen vacancies vary between 3665 and 3711 cm^{-1} . [16-17, 44] The electronically equivalent surface formed from adsorption of atomic hydrogen on the stoichiometric surface gave 3678 cm^{-1}.[18] The average value is 3686 ± 19.5 cm^{-1}. We compare this value to our calculated frequency of 3749 cm^{-1} for two equivalent bridging hydroxyls **9**, which form upon dissociative water adsorption on a vacancy site of the rutile (110) surface, and arrive at a correction factor of 0.983 ± 0.01. This scale factor is within the expected range, as discussed further in the Supporting Information.

Scaling our DFT frequencies by this factor (shown in the lower section of Figure 10) brings the anatase (001) terminal hydroxyl frequency (**1**, blue) into alignment with peak A1 and the bridging hydroxyls (**4**, **5**,**6,** purple) on (101) into agreement with peak A2. This assignment satisfies the stability constraint and the facets are known to exist on P25. A more precise scale factor can be estimated from the best fit of our frequencies (**1**, **9**, **4**, **5**,**6**) to A1, R1, and A2, which gives 0.984 ± 0.0004.

To connect our DFT results to those of Arrouvel *et al.*[20], we also need to apply an appropriate scale factor to their reported frequencies. This scale factor is expected to be closer to unity, because Arrouvel *et al.*[20] included anharmonic corrections in their calculations. Unfortunately, Arrouvel *et al.* did not calculate the frequency of bridging hydroxyls on rutile (110), which requires us to pick a different calibration point, i.e., the terminal hydroxyl **1** on the anatase (001) face, which is common to both data sets. With this reference point we estimate a scale factor of 0.988 for Arrouvel's calculated frequencies, aligning their (001) terminal hydroxyl with our A1 peak at 3717

cm^{-1}, as shown in the upper section of Figure 10. This assignment is thermally consistent. We should note that Dzwigaj *et al.*[49] assigned the band at 3735 cm^{-1} to the terminal hydroxyls on (001). However, this band is not commonly observed for pyrogenic TiO_2.[8] Busca *et al.* observed a band at 3735 cm^{-1} for anatase samples and assigned it to Si-OH hydroxyls.[81] Consistent with the latter assignment, we observed a low intensity band at 3740 cm^{-1} only when silica is detected by XPS. Therefore, we assigned the 3735 cm^{-1} band instead to Si-OH impurities.

The scaled (110) terminal hydroxyl frequency of Arrouvel *et al.*[20] could be present in low coverage, but is certainly not resolved in our spectra. The only hydroxyl close in frequency to our anatase A3 peak is the terminal hydroxyl on the (100) face, however, we observed this band after reaction with H_2, which suggests that it is more likely to be a bridging hydroxyl. These facets have been shown to exist,[43, 96] but the phase diagram[20] predicts desorption at lower temperatures. However, because the barrier to associative desorption could be sufficiently large to make it kinetically metastable (similar to the situation for the bridging hydroxyls on (101)), we cannot exclude it. Certainly other facets, such as the (112) and (103), need to be explored as potential assignments. Nevertheless, bands R2 and A3 could not be assigned definitively from the facets considered in this work.

Further support for assignment of hydroxyls A1 to terminal OH on (001) and A2 to bridging hydroxyls on (101) can be gained from the H_2 (D_2) dissociation experiments in Figures 3 and 4 where the intensity of A2 grows along with the broad electronic absorbance. Observation of a broad electronic absorbance in the difference DRIFTS spectra recorded during the reaction of H_2 with anatase and rutile samples[62] shows that electrons are transferred to the lowest unoccupied electronic states of TiO_2, which is consistent with homolytic dissociation of H_2. Homolytic dissociation of hydrogen leads to the same hydroxyl structure as water dissociation at an oxygen

vacancy site as shown in Figure 7B and C. Formation of terminal hydroxyls on the TiO_2 surfaces studied in this work upon reaction with H_2 would require breaking of a Ti-O bond, which seems unlikely. Indeed, the reaction of anatase and pyrogenic TiO_2 with H_2 did not lead to the formation of an observable A1 band, corresponding to terminal hydroxyls. Hence, we postulate that only bridging hydroxyls are formed after the reaction with H_2.

4.5 Critical assessment of methods

Although we hypothesize that the frequency of a surface hydroxyl is characteristic of a particular configuration and face, uncertainties in experiment and theory must be considered.

Instrumental accuracy and precision. The accuracy of frequencies measured by FTIR is better than 0.1 cm^{-1}, while that for HREELS is of the order 1 meV (8 cm^{-1}) due to accuracy of establishing potentials on spectrometer lens elements. Instrumental resolution in FTIR measurements of surface adsorbates is typically 4 – 8 cm^{-1} to achieve sufficient signal to noise ratio (S/N). In HREELS instrumental resolution as high as 0.5 meV have been demonstrated, however the quality of single crystal surfaces typically limits the resolution to 2-4 meV (16 – 24 cm^{-1}). The accuracy of estimating peak positions depends on peak widths, S/N, and the level of spectral processing methods used to fit complex overlapping peaks.

Theoretical accuracy and numerical precision. Although high level *ab initio* calculations (at the Møller-Plessett and configuration interaction level) with anharmonic corrections can predict experimental frequencies of small gas phase molecules with mean standard errors of ±4 cm^{-1},[97] for DFT methods, several factors are important. The magnitude of anharmonic corrections for OH stretching modes varies between 150 – 182 cm^{-1} for water, depending on the choice of functional and basis set, using second order perturbation methods.[98] For strongly intramolecular hydrogen bonded systems, the anharmonic corrections can be much larger.[99] Harmonic frequencies are

typically higher than experiment,[98, 100] but can be lower using finite difference and linear response perturbation theory methods.[101] As shown by Wei *et al*.[95] the trends in hydroxyl frequencies on different faces are reproducible, but vary systematically with functional, plane wave cutoff, choice of the Hubbard U parameter, and dipole corrections, ranging up to 150 cm^{-1} (See supporting information). For modest levels of theory, scaling harmonic frequencies achieves root mean square deviations (RMSD) of about 40 cm^{-1},[102] and anharmonic corrections may not reduce deviations.[99, 102] Numerical precision depends on factors such as k-point sampling and convergence of energy and forces, which we estimate give a RMSD of about 3 cm^{-1} (See Supporting Information). Overall, our periodic GGA+U approach with tight electronic and geometric relaxation convergence settings combined with the harmonic oscillator approximation is unlikely to give quantitative agreement with measured frequencies, but we are confident that the qualitative information from the scaled frequency values strongly supports the assignments made in this work.

Physical phenomena. Frequencies shift with temperature, coverage, and spatial configuration, which may provide additional information if their dependence is known, for example from single crystal studies or theory, but may lead to spectral broadening experimentally.

As shown in the results, thermal effects can be of order 10 cm^{-1}. The range of thermal shifts determined from experiment is indicated by the horizontal error bars in Figure 10 for anatase (A1, A2, and A3) and rutile (R1 and R2) bands. Such thermal shifts of the isolated hydroxyl bands were previously reported for the surface hydroxyls of zeolites.[8, 103-105] Several reasons, such as thermal expansion of the lattice and anharmonic effects, are proposed to explain the thermal shift of the vibrational bands.[106-108] Osuga *et al.* associated the thermal shift of the surface hydroxyls of zeolites to thermal dissociation of Brønsted acidic hydroxyls and used the degree of the shifts to calculate the ΔH of O-H dissociation.[103] The present results, as well as data in the literature,[8, 103]

show that the degree of thermal shift of surface hydroxyl bands varies among different hydroxyls on the same sample, but the shifts are smaller than the spacing between the major IR peaks.

There is limited experimental data regarding coverage dependent frequency shifts of hydroxyls on titania surfaces, and to our knowledge, only on the rutile (110). In the early work by Henderson,[16] the frequency of the hydroxyl stretch at 3690 cm^{-1} shifted downwards with increasing coverage. Yin *et al*.[18] report a frequency of 3678 cm^{-1} at the maximum observable coverage of 0.7 ML from exposure to atomic hydrogen. Our scaled theoretical frequencies for the coverage dependence on the rutile (110) surface (Table 3) predict a decrease by 30 cm^{-1} as the fraction of bridging hydroxyls occupied (for direct comparison with the experimental coverage convention) increases from 1/3 to 2/3. Therefore, theory and experiment consistently determine a red shift with increasing coverage for the bridging hydroxyls on rutile(110). Theory predicts a 12 cm^{-1} red shift also for the bridging hydroxyls (**5,6**) on anatase (101), but a blue shift of 63 cm^{-1} for bridging hydroxyls on (001), which provides no evidence for a correlation between direction of shift and oxygen coordination. The magnitude of intermolecular interactions can be assessed from the frequencies of hydroxyls **4**, **5**, and **6** shown in Figure 10, and clearly account for inhomogeneous broadening in experimental spectra.

Facet completeness. For anatase, the Wulff construction predicts that only the (101) and (001) facets would be present on the stoichiometric bulk terminated surface. The extensive work by Arrouvel *et al.*[20] examined the effect of hydroxylation on the surface energy of these and additionally the (100) and (110) faces. Because hydroxylation significantly reduced the surface energy, we considered the hydroxyls on all four surfaces they reported. Nevertheless, we have not considered all possible surface facets in our assignment. Using scanning transmission electron microscopy, Yuan *et al.* showed the presence of less common anatase surfaces such as (103),

(102), and (301) facets in anatase nanocrystals.[96] For example, Mino *et al.*[43] using DFT calculations showed that anatase (103) has a comparable energy with the anatase (001) surface, while the energy of anatase (112) is lower than the anatase (001) surface. They also suggested that the anatase (112) surface is present in the anatase particles of pyrogenic TiO_2 using FTIR of adsorbed CO.

For rutile, the Wulff construction predicts that (110) planes are most abundant, but (101), (011), (100), and (001) facets are present at equilibrium.[109] The bridging hydroxyls on the (110) surface are well known, as it is the most extensively studied single crystal oxide surface. Wei *et al*.[95] have calculated the frequency of Ti-H and bridging O-H vibrations for heterolytic dissociation of H_2 on the rutile (110), (100), (001), and (101) faces at 3607(3686), 2977(3042), 3743(3825), and 3623(3702) cm^{-1}, for the harmonic and (scaled to the bridging OH on (110) of 3686 cm^{-1}) frequencies, respectively. The frequency of the bridging hydroxyls on the rutile (101) face would probably not be resolved from the band we assigned to the terminal hydroxyls on the anatase (001) experimentally. The other hydroxyls do not account for the R2 band.

In order to assign the R2 and A3 bands, and also to be confident about the uniqueness of our assignments, the vibrational frequency of the hydroxyls on other anatase and rutile surface facets should be considered.

5 Conclusion

In this work, surface hydroxyls of pyrogenic, anatase, and rutile TiO_2 samples were studied. DRIFTS performed under a dry O_2 stream revealed the surface impurities common to the TiO_2 surfaces and the temperature at which these impurities were eliminated and enabled surface hydroxyls to be observed without carbonate and water interferences after calcination at 300 °C.

The observed bands of pyrogenic TiO_2 were a combination of anatase (A1, A2, and A3) and rutile (R1 and R2) bands, which agree well with previously reported spectra measured under dry conditions. The thermal stability of these hydroxyls assessed experimentally and on the basis of DFT calculated Gibbs free energies for dehydroxylation and dehydrogenation pathways provided additional information to assign them to terminal or bridging hydroxyls on specific facets. Additionally, after these hydroxyls were eliminated at 400 °C on P90 and rutile surfaces, reaction at 300 °C with H_2 re-formed all hydroxyls except the A1 band. The A1, A2, and A3 bands remained at 400 °C on anatase, but underwent H/D exchange upon exposure to D_2. Comparison of the "native" hydroxyls with those formed on dehydroxylated surfaces by reaction with H_2, suggests that A1 is a terminal hydroxyl while A2, A3, R1 and R2 are bridging hydroxyls. These assignments are consistent with calculated vibrational frequencies normalized to bridging hydroxyls of the rutile (110) surface and satisfy the additional criterion that the dominant peaks are assigned to hydroxyls existing on facets of low surface energy. Ultimately, we propose the following assignment of the pyrogenic TiO_2 hydroxyls bands: the 3718 cm^{-1} band is assigned to the terminal hydroxyls on the anatase (001) surface; the 3687 cm^{-1} band is assigned to the bridging hydroxyls of the rutile (110) surface; and the 3673 cm^{-1} band is assigned to the bridging hydroxyls of the anatase (101) facet.

This work has extended our understanding of the origin, thermal stability and vibrational frequency of the hydroxyls of pyrogenic TiO_2. Our DFT calculated frequencies of both terminal and bridging hydroxyls in combination with the calculated vibrational frequency of terminal hydroxyls by Arrouvel *et al.*[20] on anatase and by Wei *et al.*[95] for rutile show that the general assumption that terminal hydroxyls vibrate at higher frequencies compared to the bridging is not justified. The O-H bond length is the controlling factor in the vibrational frequency rather than the

bridging/terminal character of the hydroxyls. Surface hydroxyls of anatase (001) and anatase (101) surfaces are sufficiently resolved to allow distinguishing these two surfaces from each other. This work can potentially be used to monitor particle morphologies under working conditions and to study facet specific activity of hydroxyls in catalytic and photocatalytic conditions.

Acknowledgements

This work was supported by the U.S. National Science Foundation under award number NSF 1565843. Computational resources were provided by the uHPC cluster managed by the University of Houston and acquired through NSF-MRI award number 1531814. This work used the Extreme Science and Engineering Discovery Environment (XSEDE), which is supported by NSF grant number ACI-1053575. We also acknowledge the use of computational resources provided by the National Energy Research Scientific Computing (NERSC) Center, a DOE Office of Science User Facility supported by the Office of Science of the U.S. Department of Energy under contract number DE-AC02-05CH11231. The authors acknowledge the use of the Maxwell/Opuntia/Sabine Cluster and the advanced support from the Core facility for Advanced Computing and Data Science at the University of Houston to carry out parts of the research presented here.

Supporting Information: History and challenges of assigning surface hydroxyl frequencies on titania: early assignments of hydroxyl frequencies, challenges of oxide single crystal vibrational spectroscopy, additional complexity due to electronic defects, electronic absorption features; Additional Computational Details: surfaces used for calculations, convergence test for vibrational frequencies, scale factors for vibrational frequencies, calculations on defected surfaces; Thermodynamic Stability of Surface Hydroxyls (Electronic python notebook): Environmental assumptions for thermodynamic stability, Stability diagrams for anatase (001), anatase (101).

References

(1) Diebold, U., The Surface Science of Titanium Dioxide. *Surf. Sci. Rep.* **2003**, *48*, 53-229.

(2) Szczepankiewicz, S. H.; Colussi, A. J.; Hoffmann, M. R., Infrared Spectra of Photoinduced Species on Hydroxylated Titania Surfaces. *J. Phys. Chem. B.* **2000**, *104*, 9842-9850.

(3) Szczepankiewicz, S. H.; Moss, J. A.; Hoffmann, M. R., Electron Traps and the Stark Effect on Hydroxylated Titania Photocatalysts. *J. Phys. Chem. B.* **2002**, *106*, 7654-7658.

(4) Nanayakkara, C. E.; Pettibone, J.; Grassian, V. H., Sulfur Dioxide Adsorption and Photooxidation on Isotopically-Labeled Titanium Dioxide Nanoparticle Surfaces: Roles of Surface Hydroxyl Groups and Adsorbed Water in the Formation and Stability of Adsorbed Sulfite and Sulfate. *Phys Chem Chem Phys* **2012**, *14*, 6957-66.

(5) Deiana, C.; Fois, E.; Coluccia, S.; Martra, G., Surface Structure of TiO_2 P25 Nanoparticles: Infrared Study of Hydroxy Groups on Coordinative Defect Sites. *J. Phys. Chem. C.* **2010**, *114*, 21531-21538.

(6) Schneider, J.; Matsuoka, M.; Takeuchi, M.; Zhang, J.; Horiuchi, Y.; Anpo, M.; Bahnemann, D. W., Understanding TiO_2 Photocatalysis: Mechanisms and Materials. *Chem. Rev.* **2014**, *114*, 9919-9986.

(7) Corma, A., Inorganic Solid Acids and Their Use in Acid-Catalyzed Hydrocarbon Reactions. *Chem. Rev.***1995**, *95*, 559-614.

(8) Hadjiivanov, K., Identification and Characterization of Surface Hydroxyl Groups by Infrared Spectroscopy. In *Advances in Catalysis*, Jentoft, F.C., Ed. Academic Press:Burlington, 2014; Vol. 57, pp 99-318.

(9) Nelson, R. C.; Baek, B.; Ruiz, P.; Goundie, B.; Brooks, A.; Wheeler, M. C.; Frederick, B. G.; Grabow, L. C.; Austin, R. N., Experimental and Theoretical Insights into the Hydrogen-Efficient Direct Hydrodeoxygenation Mechanism of Phenol over Ru/TiO_2. *ACS Catal.* **2015**, *5*, 6509-6523.

(10) Thompson, T. L.; Yates, J. T., Jr. , Surface Science Studies of the Photoactivation of TiO_2 - New Photochemical Processes. *Chem. Rev.* **2006**, *106*, 4428-4453.

(11) Tykhon Zubkov; Dirk Stahl; Tracy L. Thompson; Dimitar Panayotov; Oliver Diwald; John T. Yates, J., Ultraviolet Light-Induced Hydrophilicity Effect on TiO_2(110)(1×1). Dominant Role of the Photooxidation of Adsorbed Hydrocarbons Causing Wetting by Water Droplets. *J. Phys. Chem. B* **2005**, *109*, 15454-15462.

(12) Posternak, M.; Baldereschi, A.; Delley, B., Dissociation of Water on Anatase TiO_2 Nanoparticles: The Role of Undercoordinated Ti Atoms at Edges. *J. Phys. Chem. C.* **2009**, *113*, 15862-15867.

(13) Vittadini, A.; Selloni, A.; Rotzinger, F. P.; Grätzel, M., Structure and Energetics of Water Adsorbed at TiO_2 Anatase (101) and (001) Surfaces. *Phys. Rev. Lett.* **1998**, *81*, 2954-2957.

(14) Vittadini, A.; Casarin, M.; Selloni, A., Chemistry of and on TiO_2-Anatase Surfaces by DFT Calculations: A Partial Review. *Theor. Chem. Acc.* **2007**, *117*, 663-671.

(15) Sun, C.; Liu, L.-M.; Selloni, A.; Lu, G. Q.; Smith, S. C., Titania-Water Interactions: A Review of Theoretical Studies. *J. Mater. Chem.* **2010**, *20*, 10319.

(16) Henderson, M. A., An HREELS and TPD Study of Water on TiO_2 (1l0): The Extent of Molecular Versus Dissociative Adsorption. *Surf. Sci.* **1996**, *355*, 151-166.

(17) Henderson, M. A.; Epling, W. S.; Peden, C. H. F.; Perkins, C. L., Insights into Photoexcited Electron Scavenging Processes on TiO_2 Obtained from Studies of the Reaction of O_2 with OH Groups Adsorbed at Electronic Defects on TiO_2 (110). *J. Phys. Chem. B* **2003**, *107*, 534-545.

(18) Yin, X. L.; Calatayud, M.; Qiu, H.; Wang, Y.; Birkner, A.; Minot, C.; Woll, C., Diffusion Versus Desorption: Complex Behavior of H Atoms on an Oxide Surface. *Chemphyschem* **2008**, *9*, 253-6.

(19) Brookes, I. M.; Muryn, C. A.; Thornton, G., Imaging Water Dissociation on TiO_2(110). *Phys Rev Lett* **2001**, *87*, 266103.

(20) Arrouvel, C.; Digne, M.; Breysse, M.; Toulhoat, H.; Raybaud, P., Effects of Morphology on Surface Hydroxyl Concentration: A DFT Comparison of Anatase–TiO_2 and Γ-Alumina Catalytic Supports. *J. Catal.* **2004**, *222*, 152-166.

(21) Wachs, I. E., Raman and IR Studies of Surface Metal Oxide Species on Oxide Supports: Supported Metal Oxide Catalysts. *Catal. Today* **1996**, *27*, 437-455.

(22) Lavalley, J. C., Infrared Spectrometric Studies of the Surface Basicity of Metal Oxides and Zeolites Using Adsorbed Probe Molecules. *Catal. Today* **1996**, *27*, 377-401.

(23) Mino, L.; Spoto, G.; Ferrari, A. M., CO_2 Capture by TiO_2 Anatase Surfaces: A Combined DFT and FTIR Study. *J. Phys. Chem. C.* **2014**, *118*, 25016-25026.

(24) Lercher, J. A.; Gründling, C.; Eder-Mirth, G., Infrared Studies of the Surface Acidity of Oxides and Zeolites Using Adsorbed Probe Molecules. *Catal. Today* **1996**, *27*, 353-376.

(25) Mahdavi-Shakib, A.; Husremovic, S.; Ki, S.; Glynn, J.; Babb, L.; Sempel, J.; Stavrinoudis, I.; Arce-Ramos, J. M.; Nelson, R. C.; Grabow, L. C., et al., Titania Surface Chemistry and Its Influence on Supported Metal Catalysts. *Polyhedron* **2019**, *170*, 41-50.

(26) Baertsch, C. D.; Komala, K. T.; Chua, Y.-H.; Iglesia, E., Genesis of Brønsted Acid Sites During Dehydration of 2-Butanol on Tungsten Oxide Catalysts. *J. Catal.* **2002**, *205*, 44-57.

(27) Liu, D.; Bhan, A.; Tsapatsis, M.; Al Hashimi, S., Catalytic Behavior of Brønsted Acid Sites in MWW and MFI Zeolites with Dual Meso- and Microporosity. *ACS Catal.* **2011**, *1*, 7-17.

(28) Busca, G., Acidity and Basicity of Zeolites: A Fundamental Approach. *Micropor. Mesopor. Mat.* **2017**, *254*, 3-16.

(29) Simonsen, M. E.; Li, Z.; Søgaard, E. G., Influence of the OH Groups on the Photocatalytic Activity and Photoinduced Hydrophilicity of Microwave Assisted Sol–Gel TiO_2 Film. *App. Surf. Sci.* **2009**, *255*, 8054-8062.

(30) Wu, C.-Y.; Tu, K.-J.; Deng, J.-P.; Lo, Y.-S.; Wu, C.-H., Markedly Enhanced Surface Hydroxyl Groups of TiO_2 Nanoparticles with Superior Water-Dispersibility for Photocatalysis. *Materials* **2017**, *10*, 566.

(31) Gordon, T. R.; Cargnello, M.; Paik, T.; Mangolini, F.; Weber, R. T.; Fornasiero, P.; Murray, C. B., Nonaqueous Synthesis of TiO2 Nanocrystals Using TiF_4 to Engineer Morphology, Oxygen Vacancy Concentration, and Photocatalytic Activity. *J. Am. Chem. Soc.* **2012**, *134*, 6751-6761.

(32) Wang, Y.; Wöll, C., IR Spectroscopic Investigations of Chemical and Photochemical Reactions on Metal Oxides: Bridging the Materials Gap. *Chem Soc Rev* **2017**, *46*, 1875-1932.

(33) Pellegrino, F.; Sordello, F.; Mino, L.; Minero, C.; Hodoroaba, V.-D.; Martra, G.; Maurino, V., Formic Acid Photoreforming for Hydrogen Production on Shape-Controlled Anatase TiO_2 Nanoparticles: Assessment of the Role of Fluorides, {101}/{001} Surfaces Ratio, and Platinization. *ACS Catal.* **2019**, *9*, 6692-6697.

(34) Li, D.; You, R.; Yang, M.; Liu, Y.; Qian, K.; Chen, S.; Cao, T.; Zhang, Z.; Tian, J.; Huang, W., Morphology-Dependent Evolutions of Sizes, Structures, and Catalytic Activity of Au Nanoparticles on Anatase TiO_2 Nanocrystals. *J. Phys. Chem. C* **2019**, *123*, 10367-10376.

(35) Spezzati, G.; Benavidez, A. D.; DeLaRiva, A. T.; Su, Y.; Hofmann, J. P.; Asahina, S.; Olivier, E. J.; Neethling, J. H.; Miller, J. T.; Datye, A. K., et al., CO Oxidation by Pd Supported on CeO_2(100) and CeO_2(111) Facets. *Appl. Cat. B* **2019**, *243*, 36-46.

(36) Polo-Garzon, F.; Bao, Z.; Zhang, X.; Huang, W.; Wu, Z., Surface Reconstructions of Metal Oxides and the Consequences on Catalytic Chemistry. *ACS Catal.* **2019**, *9*, 5692-5707.

(37) Hadjiivanov, K. I.; Klissurski, D. G., Surface Chemistry of Titania (Anatase) and Titania-Supported Catalysts. *Chem. Soc. Rev.* **1996**, *107*, 534-545.

(38) Newman, C.; Zhou, X.; Goundie, B.; Ghampson, I. T.; Pollock, R. A.; Ross, Z.; Wheeler, M. C.; Meulenberg, R. W.; Austin, R. N.; Frederick, B. G., Effects of Support Identity and Metal Dispersion in Supported Ruthenium Hydrodeoxygenation Catalysts. *App. Cat., A* **2014**, *477*, 64-74.

(39) Chen, H.; Nanayakkara, C. E.; Grassian, V. H., Titanium Dioxide Photocatalysis in Atmospheric Chemistry. *Chem Rev* **2012**, *112*, 5919-48.

(40) Hoffmann, M. R.; Martin, S. T.; Choi, W.; Bahnemann, D. W., Environmental Applications of Semiconductor Photocatalysis. *Chem. Rev.* **1995**, *95*, 69-96.

(41) Datye, A. K.; Riegel, G.; Bolton, J. R.; Huang, M.; Prairie, M. R., Microstructural Characterization of a Fumed Titanium Dioxide Photocatalyst. *J. Solid State Chem.* **1995**, *115*, 236-239.

(42) Ohno, T.; Sarukawa, K.; Tokieda, K.; Matsumura, M., Morphology of a TiO_2 Photocatalyst (Degussa, P-25) Consisting of Anatase and Rutile Crystalline Phases. *J. Catal.* **2001**, *203*, 82-86.

(43) Mino, L.; Spoto, G.; Bordiga, S.; Zecchina, A., Particles Morphology and Surface Properties as Investigated by HRTEM, FTIR, and Periodic DFT Calculations: From Pyrogenic TiO_2 (P25) to Nanoanatase. *J. Phys. Chem. C.* **2012**, *116*, 17008-17018.

(44) Petrik, N. G.; Kimmel, G. A., Reaction Kinetics of Water Molecules with Oxygen Vacancies on Rutile TiO_2(110). *J. Phys. Chem. C.* **2015**, *119*, 23059-23067.

(45) Hurum, D. C.; Agrios, A. G.; Gray, K. A., Explaining the Enhanced Photocatalytic Activity of Degussa P25 Mixed-Phase TiO_2 Using EPR. *J. Phys. Chem. B* **2003**, *107*, 4545-4549.

(46) Banerjee, S.; Zangiabadi, A.; Mahdavi-Shakib, A.; Husremovik, S.; Frederick, B. G.; Barmak, K.; Austin, R. N.; Billinge, S.J.L., Quantitative Structural Characterization of Catalytically Active TiO_2. Nanoparticles. **2019**, *(in press)*.

(47) Vimont, A.; Thibault-Starzyk, F.; Daturi, M., Analysing and Understanding the Active Site by IR Spectroscopy. *Chem Soc Rev* **2010**, *39*, 4928-50.

(48) Zaera, F., New Advances in the Use of Infrared Absorption Spectroscopy for the Characterization of Heterogeneous Catalytic Reactions. *Chem Soc Rev* **2014**, *43*, 7624-63.

(49) Dzwigaj, S.; Arrouvel, C.; Breysse, M.; Geantet, C.; Inoue, S.; Toulhoat, H.; Raybaud, P., DFT Makes the Morphologies of Anatase-TiO_2 Nanoparticles Visible to IR Spectroscopy. *J. Catal.* **2005**, *236*, 245-250.

(50) Michel Primet; Pierre Pichat; Mathieu, M.-V., Infrared Study of the Surface of Titanium Dioxide. I. Hydroxyl Groups. *J. Phys. Chem.* **1971**, *75*, 1216-1220.

(51) Tsyganenko, A. A.; Filimonov, V. N., Infrared Spectra of Surface Hydroxyls Groups and Crystaline Structure of Oxides. *J. Molec. Struct.* **1973**, *19*, 579-589.

(52) Panayotov, D. A.; Yates, J. T., Depletion of Conduction Band Electrons in TiO_2 by Water Chemisorption – IR Spectroscopic Studies of the Independence of Ti–OH Frequencies on Electron Concentration. *Chem. Phys. Lett.* **2005**, *410*, 11-17.

(53) Lobo-Lapidus, R. J.; Gates, B. C., Probing Surface Sites of TiO_2: Reactions with $[HRe(CO)_5]$ and $[CH_3Re(CO)_5]$. *Chemistry* **2010**, *16*, 11386-98.

(54) Lin, H.; Long, J.; Gu, Q.; Zhang, W.; Ruan, R.; Li, Z.; Wang, X., In Situ IR Study of Surface Hydroxyl Species of Dehydrated TiO_2: Towards Understanding Pivotal Surface Processes of TiO_2 Photocatalytic Oxidation of Toluene. *Phys Chem Chem Phys* **2012**, *14*, 9468-74.

(55) Liu, C.; Ma, Q.; He, H.; He, G.; Ma, J.; Liu, Y.; Wu, Y., Structure–Activity Relationship of Surface Hydroxyl Groups During NO_2 Adsorption and Transformation on TiO_2 Nanoparticles. *Environ. Sci. Nano* **2017**, *4*, 2388-2394.

(56) Rustad, J. R.; Boily, J. F., Density Functional Calculation of the Infrared Spectrum of Surface Hydroxyl Groups on Goethite (a-FeOOH). *Am. Mineral.* **2010**, *95*, 414-417.

(57) Chizallet, C.; Digne, M.; Arrouvel, C.; Raybaud, P.; Delbecq, F.; Costentin, G.; Che, M.; Sautet, P.; Toulhoat, H., Insights into the Geometry, Stability and Vibrational Properties of OH Groups on Gamma-Al_2O_3, TiO_2-Anatase and MgO from DFT Calculations. *Top. Catal.* **2009**, *52*, 1005-1016.

(58) Buchholz, M.; Xu, M.; Noei, H.; Weidler, P.; Nefedov, A.; Fink, K.; Wang, Y.; Wöll, C., Interaction of Carboxylic Acids with Rutile TiO_2(110): IR-Investigations of Terephthalic and Benzoic Acid Adsorbed on a Single Crystal Substrate. *Surf. Sci.* **2016**, *643*, 117-123.

(59) Tilocca, A.; Selloni, A., Structure and Reactivity of Water Layers on Defect-Free and Defective Anatase TiO_2(101) Surfaces. *J. Phys. Chem. B* **2004**, *108*, 4743-4751.

(60) Tilocca, A.; Selloni, A., Reaction Pathway and Free Energy Barrier for Defect-Induced Water Dissociation on the (101) Surface of TiO_2-Anatase. *J. Chem. Phys.* **2003**, *119*, 7445-7450.

(61) Nadeem, I. M.; Harrison, G. T.; Wilson, A.; Pang, C. L.; Zegenhagen, J.; Thornton, G., Bridging Hydroxyls on Anatase TiO_2(101) by Water Dissociation in Oxygen Vacancies. *J Phys Chem B* **2018**, *122*, 834-839.

(62) Mahdavi-Shakib, A.; Rahmani-Chokanlu, A.; Schwartz, T. J.; Austin, R. N.; Frederick, B. G., Implications of Electron Scavanging Character of Sulfated Titania for Photochemistry. **2019** *(in prep).*

(63) Li, G.; Li, L.; Boerio-Goates, J.; Woodfield, B. F., High Purity Anatase TiO_2 Nanocrystals: Near Room-Temperature Synthesis, Grain Growth Kinetics, and Surface Hydration Chemistry. *J. Am. Chem. Soc.* **2005**, *127*, 8659-8666.

(64) Kresse, G.; Furthmüller, J., Efficiency of Ab-Initio Total Energy Calculations for Metals and Semiconductors Using a Plane-Wave Basis Set. *Comput. Mater. Sci.* **1996**, *6*, 15-50.

(65) Kresse, G.; Hafner, J., Ab Initio Molecular Dynamics for Open-Shell Transition Metals. *Phys. Rev. B* **1993**, *48*, 13115-13118.

(66) Kresse, G.; Hafner, J., Ab Initio Molecular-Dynamics Simulation of the Liquid-Metal--Amorphous-Semiconductor Transition in Germanium. *Phys. Rev. B* **1994**, *49*, 14251-14269.

(67) Hjorth Larsen, A.; Jørgen Mortensen, J.; Blomqvist, J.; Castelli, I. E.; Christensen, R.; Dułak, M.; Friis, J.; Groves, M. N.; Hammer, B.; Hargus, C., et al., The Atomic Simulation Environment—a Python Library for Working with Atoms. *J. Phys. Condens. Matter* **2017**, *29*, 273002.

(68) Blöchl, P. E., Projector Augmented-Wave Method. *Phys. Rev. B* **1994**, *50*, 17953-17979.

(69) Hammer, B.; Hansen, L. B.; Nørskov, J. K., Improved Adsorption Energetics within Density-Functional Theory Using Revised Perdew-Burke-Ernzerhof Functionals. *Phys. Rev. B* **1999**, *59*, 7413-7421.

(70) Perdew, J. P.; Burke, K.; Ernzerhof, M., Generalized Gradient Approximation Made Simple. *Phys. Rev. Lett.* **1996**, *77*, 3865-3868.

(71) Blöchl, P. E.; Jepsen, O.; Andersen, O. K., Improved Tetrahedron Method for Brillouin-Zone Integrations. *Phys. Rev. B* **1994**, *49*, 16223-16233.

(72) Dudarev, S. L.; Botton, G. A.; Savrasov, S. Y.; Humphreys, C. J.; Sutton, A. P., Electron-Energy-Loss Spectra and the Structural Stability of Nickel Oxide: An LSDA+U Study. *Phys. Rev. B* **1998**, *57*, 1505-1509.

(73) Hu, Z.; Metiu, H., Choice of U for DFT+U Calculations for Titanium Oxides. *J. Phy. Chem. C* **2011**, *115*, 5841-5845.

(74) Arlt, T.; Bermejo, M.; Blanco, M. A.; Gerward, L.; Jiang, J. Z.; Staun Olsen, J.; Recio, J. M., High-Pressure Polymorphs of Anatase TiO_2. *Phys. Rev. B* **2000**, *61*, 14414-14419.

(75) Morgan, B. J.; Watson, G. W., A Density Functional Theory + U Study of Oxygen Vacancy Formation at the (110), (100), (101), and (001) Surfaces of Rutile TiO_2. *J. Phys. Chem. C.* **2009**, *113*, 7322-7328.

(76) Chueh, Y.-L.; Hsieh, C.-H.; Chang, M.-T.; Chou, L.-J.; Lao, C. S.; Song, J. H.; Gan, J.-Y.; Wang, Z. L., RuO_2 Nanowires and RuO_2/TiO_2 Core/Shell Nanowires: From Synthesis to Mechanical, Optical, Electrical, and Photoconductive Properties. *Adv. Mater.* **2007**, *19*, 143-149.

(77) Bengtsson, L., Dipole Correction for Surface Supercell Calculations. *Phys. Rev. B* **1999**, *59*, 12301-12304.

(78) Monkhorst, H. J.; Pack, J. D., Special Points for Brillouin-Zone Integrations. *Phys. Rev. B* **1976**, *13*, 5188-5192.

(79) Porezag, D.; Pederson, M. R., Infrared Intensities and Raman-Scattering Activities within Density-Functional Theory. *Phys. Rev. B* **1996**, *54*, 7830-7836.

(80) Mino, L.; Spoto, G.; Bordiga, S.; Zecchina, A., Rutile Surface Properties Beyond the Single Crystal Approach: New Insights from the Experimental Investigation of Different Polycrystalline Samples and Periodic DFT Calculations. *J. Phy. Chem. C* **2013**, *117*, 11186-11196.

(81) Busca, G.; Saussey, H.; Saur, O.; Lavalley, J. C.; Lorenzelli, V., FT-IR Characterization of the Surface Acidity of Different Titanium Dioxide Anatase Preparations. *Appl. Catal.A* **1985**, *14*, 245-260.

(82) Šurca Vuk, A.; Ješe, R.; Gaberšček, M.; Orel, B.; Dražič, G., Structural and Spectroelectrochemical (UV–vis and IR) Studies of Nanocrystalline Sol–Gel Derived TiO_2 Films. *Sol. Energ. Mat. Sol. C.* **2006**, *90*, 452-468.

(83) Lewis, K. E.; Parfit, G. D., Infra-Red Study of the Surface of Rutile. *J. Chem. Soc. Farad. Trans.* **1966**, *62*, 204-214.

(84) McCool, B.; Tripp, C. P., Inaccessible Hydroxyl Groups on Silica Are Accessible in Supercritical CO_2. *J. Phys. Chem. B* **2005**, *109*, 8914-8919.

(85) Han, B.; Hang Hu, Y., Investigation on H-Containing Shallow Trap of Hydrogenated TiO_2 with in-situ Fourier Transform Infrared Diffuse Reflection Spectroscopy. *Nanotechnology* **2017**, *28*, 304001.

(86) Panayotov, D.; Ivanova, E.; Mihaylov, M.; Chakarova, K.; Spassov, T.; Hadjiivanov, K., Hydrogen Spillover on Rh/TiO_2: The FTIR Study of Donated Electrons, Co-adsorbed CO and H/D Exchange. *Phys Chem Chem Phys* **2015**, *17*, 20563-73.

(87) Panayotov, D. A.; Burrows, S. P.; Morris, J. R., Infrared Spectroscopic Studies of Conduction Band and Trapped Electrons in UV-Photoexcited, H-Atom N-Doped, and Thermally Reduced TiO_2. *J. Phys. Chem. C.* **2012**, *116*, 4535-4544.

(88) Sezen, H.; Buchholz, M.; Nefedov, A.; Natzeck, C.; Heissler, S.; Di Valentin, C.; Wöll, C., Probing Electrons in TiO_2 Polaronic Trap States by IR-Absorption: Evidence for the Existence of Hydrogenic States. *Sci. Rep.* **2014**, *4*, 3808.

(89) Chase, M. W., *NIST-JANAF Themochemical Tables*, 4th ed.; J. Phys. Chem. Ref. Data Monographs, American Institute of Physics: 1998; Vol. 9.

(90) Bredow, T.; Jug, K., Theoretical Investigation of Water-Adsorption at Rutile and Anatase Surfaces. *Surf. Sci.* **1995**, *327*, 398-408.

(91) Erdogan, R.; Onal, I., An ONIOM and DFT Study of Water and Ammonia Adsorption on Anatase TiO_2(001) Cluster. *Int. J. Quant. Chem.* **2011**, *111*, 2149-2159.

(92) Aschauer, U.; Selloni, A., Hydrogen Interaction with the Anatase TiO_2(101) Surface. *Phys Chem Chem Phys* **2012**, *14*, 16595-602.

(93) De Angelis, F.; Di Valentin, C.; Fantacci, S.; Vittadini, A.; Selloni, A., Theoretical Studies on Anatase and Less Common TiO_2 Phases: Bulk, Surfaces, and Nanomaterials. *Chem Rev* **2014**, *114*, 9708-53.

(94) Henderson, M. A.; Lyubinetsky, I., Molecular-Level Insights into Photocatalysis from Scanning Probe Microscopy Studies on TiO_2 (110). *Chem. Rev.* **2013**, *113*, 4428-55.

(95) Wei, B.; Tielens, F.; Calatayud, M., Understanding the Role of Rutile TiO_2 Surface Orientation on Molecular Hydrogen Activation. *Nanomaterials* **2019**, *9*, 1199.

(96) Yuan, W.; Meng, J.; Zhu, B.; Gao, Y.; Zhang, Z.; Sun, C.; Wang, Y., Unveiling the Atomic Structures of the Minority Surfaces of TiO_2 Nanocrystals. *Chem. Mater.* **2018**, *30*, 288-295.

(97) Rauhut, G.; Barone, V.; Schwerdtfeger, P., Vibrational Analyses for CHFClBr and CDFClBr Based on High Level Ab Initio Calculations. *J. Chem. Phys.* **2006**, *125*, 054308.

(98) Barone, V., Anharmonic Vibrational Properties by a Fully Automated Second-Order Perturbative Approach. *J. Chem. Phys.* **2005**, *122*, 014108.

(99) Spanget-Larsen, J.; Hansen, B. K. V.; Hansen, P. E., OH Stretching Frequencies in Systems with Intramolecular Hydrogen Bonds: Harmonic and Anharmonic Analyses. *Chem. Phys.* **2011**, *389*, 107-115.

(100) Giannozzi, P.; Baroni, S., Vibrational and Dielectric Properties of C60 from Density-Functional Perturbation Theory. *J. Chem. Phys.* **1994**, *100*, 8537-8539.

(101) Putrino, A.; Sebastiani, D.; Parrinello, M., Generalized Variational Density Functional Perturbation Theory. *J. Chem. Phys.* **2000**, *113*, 7102-7109.

(102) Jacobsen, R. L.; Johnson, R. D.; Irikura, K. K.; Kacker, R. N., Anharmonic Vibrational Frequency Calculations Are Not Worthwhile for Small Basis Sets. *J. Chem. Theory Comput.* **2013**, *9*, 951-954.

(103) Osuga, R.; Yokoi, T.; Doitomi, K.; Hirao, H.; Kondo, J. N., Infrared Investigation of Dynamic Behavior of Brønsted Acid Sites on Zeolites at High Temperatures. *J. Phys. Chem. C* **2017**, *121*, 25411-25420.

(104) Miki Niwa; Katsuki Suzuki; Kazuyo Isamoto; Katada, N., Identification and Measurements of Strong Brønsted Acid Site in Ultrastable Y (USY) Zeolite. *J. Phys. Chem. B* **2006**, *110*, 264-269.

(105) Miki Niwa; Katsuki Suzuki; Naonobu Katada; Tomonori Kanougi; Atoguchi, T., Ammonia IRMS-TPD Study on the Distribution of Acid Sites in Mordenite. *J. Phys. Chem. B* **2005**, *109*, 18749-18757.

(106) Mondal, T.; Tripathi, A.; Zhang, J.; Sathe, V.; Shripathi, T.; Shinohara, H.; Tiwari, A., Temperature-Dependent Raman Study of Gd@C82. *J. Phys. Chem. C* **2015**, *119*, 12698-12702.

(107) Yiqing, C.; Peng, B.; Wang, B., Raman Spectra and Temperature-Dependent Raman Scattering of Silicon Nanowires. *J. Phys. Chem. C* **2007**, *111*, 5855-5858.

(108) Mendoca, C.; Rabbani, S. R., Anharmonic Lattice Vibrations and the Temperature Shift of Raman Spectra. *Z. Naturforsch* **1996**, *51a*, 716-720.

(109) Ramamoorthy, M.; Vanderbilt, D.; King-Smith, R. D., First-Principles Calculations of the Energetics of Stoichiometric TiO_2 Surfaces. *Phys. Rev. B* **1994**, *49*, 16721-16727.

TOC Graphic:

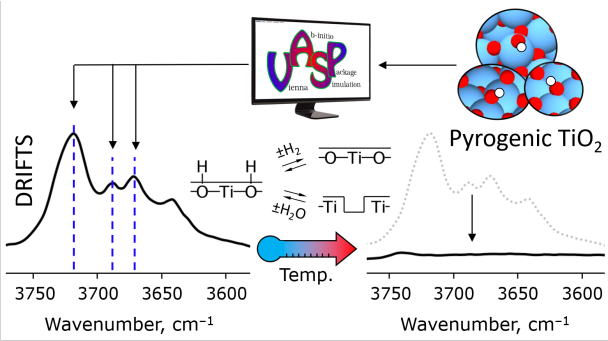
DRIFTS
Pyrogenic TiO2
Temp.
3750 3700 3650 3600
Wavenumber, cm-1
3750 3700 3650 3600
Wavenumber, cm-1